Analogs of quantum-Hall-effect edge states in photonic crystals

S. Raghu*
Department of Physics, Stanford University, Stanford, California 94305-4045, USA

F. D. M. Haldane
Department of Physics, Princeton University, Princeton, New Jersey 08544-0708, USA
(Received 14 April 2008; published 23 September 2008)

Photonic crystals built with time-reversal-symmetry-breaking Faraday-effect media can exhibit chiral edge modes that propagate unidirectionally along boundaries across which the Faraday axis reverses. These modes are precise analogs of the electronic edge states of quantum-Hall-effect (QHE) systems, and are also immune to backscattering and localization by disorder. The Berry curvature of the photonic bands plays a role analogous to that of the magnetic field in the QHE. Explicit calculations demonstrating the existence of such unidirectionally propagating photonic edge states are presented.

DOI: 10.1103/PhysRevA.78.033834 PACS number(s): 42.70.Qs, 03.65.Vf

I. INTRODUCTION

The control of the flow of light using photonic-band-gap (PBG) materials has received considerable attention over the past decade [1]. Moreover, the potential for using artificially structured metamaterials, such as the recently discovered left-handed media [2], has shown considerable technological promise. In the past, significant progress has been achieved in the field of photonics by making use of analogies with electronic systems. For instance, the idea of a PBG material, a system with a spatially varying and periodic dielectric function, was motivated by the well-known physics of electronic Bloch states; the dielectric scattering of light in periodic media presents the same formal solutions as those for the scattering of electrons in periodic potentials.

Previous photonic-band-structure calculations have focused on the frequency dispersion of the photon bands; it has been usually been assumed that a knowledge of the spectrum alone represents a complete understanding of the dynamics of the system. A primary goal of such calculations has been the quest for a PBG material with a complete band gap throughout the Brillouin zone in some frequency range, which would prevent the transmission of light with frequency in the range of the band gap. Both two- and three-dimensional band structures possessing these properties have now been discovered [3].

Recently, however, in the study of electronic systems, it has become apparent that, even in the absence of interaction effects, the dispersion relations of the energy bands do not fully characterize the semiclassical dynamics of wave packets, unless both spatial-inversion symmetry and time-reversal symmetry are unbroken [4]. The additional information, which is not obtainable from knowledge of the energy bands $\epsilon_n(\boldsymbol{k})$ alone, is the variation of the Berry curvature [5] $\mathcal{F}_n^{ab}(\boldsymbol{k})=\epsilon^{abc}\Omega_{nc}(\boldsymbol{k})$, which is an antisymmetric tensor in $\boldsymbol{k}$ space, where $\Omega_n(\boldsymbol{k})$ is analogous to a magnetic field (flux density) in $\boldsymbol{k}$ space. The Berry curvature in $\boldsymbol{k}$ space is related to the Berry phase [6] in the same way that the Bohm-Aharonov phase of an electronic wave packet is related to the magnetic flux density in real space.

While the uniform propagation of wave packets in perfectly translationally invariant systems does not involve the Berry curvature, the semiclassical description of the *acceleration* of wave packets in media with spatial inhomogeneity of length scales large compared to the underlying lattice spacing is incomplete if it is not taken into account. Recently, Onoda *et al.* [7] have pointed out the role of Berry curvature in photonic crystals without inversion symmetry; while these authors characterize this as a "Hall effect of light," the Hall effect in electronic systems is associated with broken *time-reversal symmetry* rather than, broken spatial-inversion symmetry, and we have recently discussed [8] some of the effects at first sight surprising, that broken time-reversal symmetry could produce in photonic systems.

In the presence of nonvanishing Berry curvature, the usual semiclassical expression for the group velocity of the wave packet is supplemented by an additional anomalous contribution proportional to its acceleration and the local Berry curvature of the Bloch band. (The semiclassical treatment of electron dynamics becomes ray optics in the photonic context.) This anomalous velocity has played an important role in understanding recent experiments on the anomalous Hall effect of ferromagnets [9], for example.

Perhaps the most remarkable among the "exotic" effects associated with Berry curvature, however, is the quantum Hall effect [10], which has been the focus of intensive experimental and theoretical study in condensed matter physics for over two decades. The physics of the quantum Hall regime and its connection with Berry curvature phenomena is now well understood. The possibility of transcribing some of the main features of the quantum Hall effect to photonic systems, which brings into play new possibilities in photonics, is the topic of this paper. Specifically, we shall concern ourselves with analogs of "chiral" (unidirectional) quantum Hall edge states in photonic systems with broken time-reversal symmetry.

The quantum Hall effect is usually associated with two-dimensional electron systems in semiconductor heterojunctions in strong applied magnetic fields. By treating the plane of the heterojunction as a featureless two-dimensional (2D)

*sraghu@stanford.edu

continuum, and considering the quantum mechanical motion of electrons in the presence of a magnetic field, one obtains the electronic Landau levels. The key feature giving rise to the quantization of the Hall conductance is the incompressibility of the electron fluid, due to the Pauli principle at either integer Landau level fillings, with the spectral gap to the next empty level given by the cyclotron frequency, or at fractional fillings when a gap opens due to strong electron-electron interactions [11].

While in the experimentally realized systems the quantum Hall effect derives from a strong uniform component of the magnetic flux density normal to the 2D plane in which the electrons move, the integer quantum Hall effect can also in principle derive from the interplay of a periodic band structure with a magnetic field. Magnetic fields externally applied in periodic structures give rise to the celebrated Hofstadter model of Bloch bands with an elegant fractal spectral structure depending on the rational value of the magnetic flux through the unit cell [12,13]. The influence of the lattice on the quantum Hall effect was further investigated in an important paper by Thouless, Kohmoto, Nightingale, and den Nijs (TKNN) [14], who discovered a topological invariant of 2D band structures known as the "Chern number," a quantity that was later interpreted in terms of Berry curvature [5].

At first sight, it seems implausible that any of the phenomena associated with the quantum Hall effect can be transcribed to photonics. Incompressibility and Landau level quantization require fermions and charged particles, respectively, and it is not clear how one could introduce an effect similar to the Lorentz force due to a magnetic field on a system of neutral bosons. However, a hint that possible analogs could exist in photonics comes from the fact that a zero-field quantum Hall effect *without any net magnetic flux density* (and hence without Landau levels) could occur in systems consisting of "simple" Bloch states with broken time-reversal symmetry, as was shown some time ago by one of us [15]. The explicit "graphenelike" model investigated in Ref. [15] exploits the topological properties of Bloch states, which motivated us to construct its photonic counterpart. This model has also turned out to be very useful for modeling the anomalous Hall effect in ferromagnetic metals [16], and a recently proposed "quantum spin Hall effect" [17].

While incompressibility of the fluid in the bulk quantizes the Hall conductance, perhaps the most remarkable feature of quantum Hall systems is the presence of zero-energy excitations along the *edge* of a finite system. In these edge states, electrons travel along a single direction: this one-way propagation is a symptom of broken time-reversal symmetry. In the case that the integer quantum Hall effect is exhibited by Bloch electrons, as in the Hofstadter problem studied by TKNN [14], it is related to the topological Chern invariant of the one-particle bands. The edge states necessarily occur at the interface between bulk regions in which there is a gap at the Fermi energy, which have different values of the sum of the Chern invariants of the fully occupied bands below the Fermi level. While the integer quantum Hall effect in such a system itself involves the filling of these bands according to the Pauli principle, and hence is essentially fermionic in nature, the existence of the edge states is a property of the one-electron band structure, without reference to the Pauli principle, which suggests that this feature is not restricted to fermionic systems. We have found that they indeed have a direct photonic counterpart, and this leads to the idea that topologically nontrivial *unidirectionally propagating photon modes* can occur along domain walls separating two PBG regions having different Chern invariants of bands below the band gap frequency. In this paper, we present the formal basis of such modes, along with explicit numerical examples, simple model Hamiltonians, and semiclassical calculations confirming the concept.

We note, finally, that while nowadays the Berry phase is usually associated with quantum mechanical interference it can in principle occur wherever phase interference phenomena exist and are governed by Hermitian eigenvalue problems, as in the case of classical electromagnetic waves in loss-free media. Indeed, the idea of the geometric phase was originally proposed in the context of classical optics [18] several decades before being introduced into quantum mechanics.

This paper is organized as follows. In Sec. II, we present the basic formalism of the Maxwell normal mode problem in periodic, loss-free media, discuss the Berry curvature of the photonic-band-structure problem, and consider the effects of broken time-reversal symmetry. In Sec. III, we provide explicit numerical examples of band structures containing nontrivial topological properties, and show the occurrence of edge states along domain wall configurations. Motivated by the numerical results, in Sec. IV, we derive a simple Dirac Hamiltonian from the Maxwell equations using symmetry arguments as the guiding principle, and we show how under certain conditions the *zero modes* of this Dirac Hamiltonian exhibit anomalous currents along a single direction due to the breaking of time-reversal symmetry. It is these zero modes that play the role of the "gapless" edge excitations, as we shall consider in detail. Section V contains a semiclassical analysis, and we end with a discussion and point out possible future directions in Sec. VI.

II. BERRY CURVATURE IN THE MAXWELL NORMAL MODE PROBLEM

In this section, we discuss the formal basis of Berry curvature in the photon band problem. We begin with the basic formulation of the photonic-band-structure problem, which is somewhat more complicated than the electronic counterpart, due to the frequency response of dielectric media. We then briefly review the connection between Chern numbers, Berry curvature, and the occurrence of gapless edge modes along the boundary where the Chern numbers of a given band change.

A. Basic formalism

We will be solving the source-free Maxwell equations for propagating electromagnetic wave solutions in linear, loss-free media, and will ignore absorption, nonlinear photon-photon interactions, and other processes that do not conserve photon number. We also assume that the constitutive relations, reflecting the response of the media to the electromag-

netic waves, are given by local, but spatially varying, tensors with generalized frequency dependence. The Berry phase, and the associated Berry curvature, are commonly identified with quantum mechanics, but in fact are more generally associated with the adiabatic variation of the complex eigenvectors of a Hermitian eigenvalue system as the Hermitian matrix is varied.

In quantum mechanics, this Hermitian eigenvalue problem is the time-independent Schrödinger equation; in the photonic context, it is the classical eigenvalue equation for the normal modes of the Maxwell equations. In order to make the correspondence with the standard quantum mechanical formulation of Berry curvature clearer, we will use a somewhat unfamiliar Hamiltonian formulation of Maxwell's equations, which is appropriate for loss-free linear media. However, we should emphasize that our results are in no way dependent on the use of such a formalism, and are properties of the Maxwell equations, however they are written.

In such a loss-free, linear medium, the coupling of electromagnetic modes having different frequencies can be ignored, and the electromagnetic fields and flux densities $\boldsymbol{X}(\boldsymbol{r},t)$, $\boldsymbol{X}\in\{\boldsymbol{D},\boldsymbol{B},\boldsymbol{E},\boldsymbol{H}\}$, will be of the form

$$\boldsymbol{X}(\boldsymbol{r},t)=[\tilde{\boldsymbol{X}}^{*}(\boldsymbol{r},\omega)e^{i\omega t}+\tilde{\boldsymbol{X}}(\boldsymbol{r},\omega)e^{-i\omega t}], \tag{1}$$

where the quantities $\tilde{\boldsymbol{X}}$ are in general complex-valued functions of position and frequency with the property

$$[\tilde{\boldsymbol{X}}(\boldsymbol{r},\omega)]^{*}=\tilde{\boldsymbol{X}}(\boldsymbol{r},-\omega). \tag{2}$$

The dynamics of these fields are governed by the source-free Maxwell equations

$$\boldsymbol{\nabla}\times\tilde{\boldsymbol{E}}=i\omega\tilde{\boldsymbol{B}},\quad \boldsymbol{\nabla}\times\tilde{\boldsymbol{H}}=-i\omega\tilde{\boldsymbol{D}}, \tag{3}$$

$$\boldsymbol{\nabla}\cdot\tilde{\boldsymbol{D}}=0,\quad \boldsymbol{\nabla}\cdot\tilde{\boldsymbol{B}}=0. \tag{4}$$

Consider a single normal mode λ propagating at frequency ω_{λ}. For the moment, ignore any internal polarization or magnetization modes of the medium, and assume instantaneous frequency-independent response of the dielectric material. In this limit, the permeability and permittivity tensors, defined by the relations

$$\tilde{B}^{a}(\boldsymbol{r},\omega_{\lambda})=\mu^{ab}(\boldsymbol{r})\tilde{H}_{b}(\boldsymbol{r},\omega_{\lambda}), \tag{5}$$

$$\tilde{D}^{a}(\boldsymbol{r},\omega_{\lambda})=\epsilon^{ab}(\boldsymbol{r})\tilde{E}_{b}(\boldsymbol{r},\omega_{\lambda}), \tag{6}$$

are both positive-definite Hermitian tensors and have well-defined, positive-definite Hermitian inverses $\epsilon^{-1}_{ab}(\boldsymbol{r})$, $\mu^{-1}_{ab}(\boldsymbol{r})$. Since we have assumed a linear, loss-free medium in which photon number is conserved, it is convenient to work with a Hamiltonian formalism: the time-averaged energy density of the electromagnetic radiation field is given by

$$\mathcal{H}^{\mathrm{EM}}(\boldsymbol{r})=u^{e}(\boldsymbol{r})+u^{m}(\boldsymbol{r}), \tag{7}$$

where

$$u^{e}(\boldsymbol{r})=\frac{1}{2}(\tilde{\boldsymbol{D}}^{*}_{\lambda},\epsilon^{-1}(\boldsymbol{r})\tilde{\boldsymbol{D}}_{\lambda}), \tag{8}$$

$$u^{m}(\boldsymbol{r})=\frac{1}{2}(\tilde{\boldsymbol{B}}^{*}_{\lambda},\mu^{-1}(\boldsymbol{r})\tilde{\boldsymbol{B}}_{\lambda}), \tag{9}$$

and the parentheses denote contraction over the spatial components of the normal mode fields. Then, if H^{EM} is the spatial integral of the energy density, the fields $\boldsymbol{E}$ and $\boldsymbol{H}$ are given by its functional derivatives with respect to the divergence-free flux densities $\boldsymbol{D}$ and $\boldsymbol{B}$:

$$\delta H^{\mathrm{EM}}=\int d^{3}\boldsymbol{r}\, E_{a}\delta B^{a}+H_{a}\delta B^{a}. \tag{10}$$

In the local Hamiltonian formalism, the flux density fields $\boldsymbol{D}(\boldsymbol{r})$ and $\boldsymbol{B}(\boldsymbol{r})$ are the fundamental degrees of freedom, and they obey the following noncanonical Poisson bracket relations:

$$\{D^{a}(r),B^{b}(r')\}_{\mathrm{PB}}=\epsilon^{abc}\boldsymbol{\nabla}_{c}\delta^{3}(r-r'). \tag{11}$$

This Poisson bracket generates the Faraday-Maxwell equations (3):

$$\frac{d\boldsymbol{D}}{dt}=\{\boldsymbol{D}(\boldsymbol{r}),H^{\mathrm{EM}}\}_{\mathrm{PB}},\quad \frac{d\boldsymbol{B}}{dt}=\{\boldsymbol{B}(\boldsymbol{r}),H^{\mathrm{EM}}\}_{\mathrm{PB}}. \tag{12}$$

Note that these equations do *not* generate the Gauss law equations (4), but merely ensure that any divergences $\boldsymbol{\nabla}_{a}D^{a}$ and $\boldsymbol{\nabla}_{a}B^{a}$ are constants of the motion; the Gauss laws are additional constraints that are compatible with the Faraday-Maxwell equations of motion.

If internal polarization and magnetization modes of the medium are ignored, a discretized form of the electromagnetic Hamiltonian is formally identical in structure to that of a collection of real oscillator variables x_{i} with noncanonical Poisson brackets

$$\{x_{i},x_{j}\}_{\mathrm{PB}}=S_{ij}, \tag{13}$$

where S_{ij} is a real antisymmetric matrix, and the Hamiltonian energy function is

$$\mathcal{H}=\frac{1}{2}\sum_{ij}B_{ij}x_{i}x_{j}, \tag{14}$$

where B_{ij} is a real symmetric positive-definite matrix. It is useful to introduce the imaginary antisymmetric Hermitian matrix $A_{ij}=iS_{ij}$. The canonical normal modes are given by

$$q_{\lambda}\pm ip_{\lambda}=(\gamma_{\lambda})^{-1}\sum_{i}u^{\pm}_{i\lambda}x_{i}, \tag{15}$$

where γ_{λ} is an arbitrary scale factor, and where $(u^{\sigma}_{i\lambda})^{*}=u^{-\sigma}_{i\lambda}$, $\sigma=\pm$, which obeys the generalized Hermitian eigenvalue equation

$$\sum_{j}A_{ij}u^{\pm}_{j\lambda}=\pm\omega_{\lambda}\sum_{j}B^{-1}_{ij}u^{\pm}_{j\lambda} \tag{16}$$

with $\omega_{\lambda}>0$, and the orthogonality condition

$$\sum_{ij}(u^{\sigma}_{i\lambda})^{*}B^{-1}_{ij}u^{\sigma'}_{j\lambda'}=\frac{\gamma^{2}_{\lambda}}{\omega_{\lambda}}\delta_{\sigma\sigma'}\delta_{\lambda\lambda'}. \tag{17}$$

Because of the antisymmetric Hermitian property of the matrix A_{ij} and the positive-definite real symmetric property of

the matrix B_{ij}, this eigenproblem has real eigenvalues that either come in pairs $\pm\omega_\lambda$, or vanish; these equations provide a straightforward transformation to canonical form only if the generalized eigenvalue problem has no zero-frequency eigenvalues, which is the case only if A_{ij} is nonsingular.

The coefficients $u_{i\lambda}$ are the analogs of the electromagnetic fields $\tilde{E}(\boldsymbol{r},\omega)$ and $\tilde{H}(\boldsymbol{r},\omega)$. It is also useful to introduce the conjugate quantities

$$v_{i\lambda}^{\sigma} = \sum_j B_{ij}^{-1} u_{j\lambda}^{\sigma}, \quad \sum_i (v_{i\lambda}^{\sigma})^* u_{i\lambda'}^{\sigma'} = \delta_{\sigma\sigma'}\delta_{\lambda\lambda'}; \tag{18}$$

these are the analogs of the flux densities $\tilde{\boldsymbol{D}}(\boldsymbol{r},\omega)$ and $\tilde{\boldsymbol{B}}(\boldsymbol{r},\omega)$, and B_{ij} encodes the "constitutive relations" between analogs of fluxes and fields.

The Hamiltonian formulation of the Maxwell equations indeed presents the difficulty of having a null space of zero-frequency eigenvalues: by themselves, the Faraday-Maxwell equations have static (zero-frequency) solutions $\tilde{\boldsymbol{B}}(\boldsymbol{r}) = \boldsymbol{\nabla} f(\boldsymbol{r})$, $\tilde{\boldsymbol{D}}(\boldsymbol{r}) = \boldsymbol{\nabla} g(\boldsymbol{r})$; the role of the additional Gauss law constraints is precisely to eliminate these zero modes. The zero-mode problem in the Hamiltonian formulation is the counterpart of the gauge ambiguity of the solutions of Maxwell's equations in the Lagrangian formulation.

In the Maxwell equations, B_{ij} becomes the following positive-definite 6×6 Hermitian matrix:

$$B_{ij} \to \begin{pmatrix} \epsilon_{ab}^{-1}(\boldsymbol{r}) & 0 \\ 0 & \mu_{ab}^{-1}(\boldsymbol{r}) \end{pmatrix}. \tag{19}$$

More precisely, this is a 6×6 block of an infinite-dimensional "matrix" that is block diagonal in terms of the spatial coordinate $\boldsymbol{r}$. (The A and B matrix notation is common in the context of generalized Hermitian eigenvalue problems, where the positive-definite character of the B matrix guarantees reality of the eigenvalues; hopefully the context should distinguish our use of the symbol B for such a matrix from the symbol $\boldsymbol{B}(\boldsymbol{r})$ used for the magnetic flux density.) In this continuum limit, the antisymmetric Hermitian matrix A_{ij} becomes a 6×6 matrix block of differential operators:

$$A^{ac} = \begin{pmatrix} 0 & i\epsilon^{abc}\boldsymbol{\nabla}_b \\ -i\epsilon^{abc}\boldsymbol{\nabla}_b & 0 \end{pmatrix}. \tag{20}$$

This A matrix can also be elegantly expressed using the 3×3 spin-1 matrix representations of the angular momentum algebra, $(L^b)^{ac} = i\epsilon^{abc}$:

$$A = \begin{pmatrix} 0 & \boldsymbol{L}^a\boldsymbol{\nabla}_a \\ -\boldsymbol{L}^a\boldsymbol{\nabla}_a & 0 \end{pmatrix}. \tag{21}$$

From the antisymmetry of A, it again follows that its eigenvalues either come in $\pm$ pairs, or are zero modes, corresponding to static field configurations. Due to the presence of a huge band of zero modes (one-third of the spectrum), the A matrix cannot be written in canonical form.

Using the Poisson brackets, we see that the equation of motion of the electric and magnetic fields is a generalized Hermitian eigenvalue problem of the form

$$\begin{pmatrix} 0 & \boldsymbol{L}^a\boldsymbol{\nabla}_a \\ -\boldsymbol{L}^a\boldsymbol{\nabla}_a & 0 \end{pmatrix} \begin{bmatrix} \tilde{\boldsymbol{E}}_\lambda \\ \tilde{\boldsymbol{H}}_\lambda \end{bmatrix} = \omega_\lambda \begin{pmatrix} \boldsymbol{\epsilon}(\boldsymbol{r}) & 0 \\ 0 & \boldsymbol{\mu}(\boldsymbol{r}) \end{pmatrix} \begin{bmatrix} \tilde{\boldsymbol{E}}_\lambda \\ \tilde{\boldsymbol{H}}_\lambda \end{bmatrix}.$$

In this formalism, the energy density of the normal mode (time averaged over the periodic cycle) is

$$u(\boldsymbol{r}) = \frac{1}{2}[\tilde{\boldsymbol{E}}_\lambda^* \quad \tilde{\boldsymbol{H}}_\lambda^*] \begin{pmatrix} \boldsymbol{\epsilon}(\boldsymbol{r}) & 0 \\ 0 & \boldsymbol{\mu}(\boldsymbol{r}) \end{pmatrix} \begin{bmatrix} \tilde{\boldsymbol{E}}_\lambda \\ \tilde{\boldsymbol{H}}_\lambda \end{bmatrix}, \tag{22}$$

and the period-averaged energy-current density (Poynting vector) is

$$j^a(\boldsymbol{r}) = \frac{1}{2}[\tilde{\boldsymbol{E}}_\lambda^* \quad \tilde{\boldsymbol{H}}_\lambda^*] \begin{pmatrix} 0 & -i\boldsymbol{L}^a \\ i\boldsymbol{L}^a & 0 \end{pmatrix} \begin{bmatrix} \tilde{\boldsymbol{E}}_\lambda \\ \tilde{\boldsymbol{H}}_\lambda \end{bmatrix}. \tag{23}$$

For practical real-space-based calculations of the photonic normal mode spectrum with inhomogeneous local constitutive relations, it is very convenient to discretize the continuum Maxwell equations on a lattice (or network) in such a way that they in fact have the matrix form (16), where the matrix A_{ij} reproduces the zero-mode (null-space) structure of the continuum equations, and H_{ij} represents the local constitutive relations at network nodes (which come in dual types, electric and magnetic). In such a scheme, divergence-free electric and magnetic fluxes flow along the links of the interpenetrating dual electric and magnetic networks, while electromagnetic energy flows between electric and magnetic nodes, along the links between nodes of the network, satisfying a local continuity equation (see Appendix B). However, there is one further conceptual ingredient that needs to be added to the formalism before we can discuss the Maxwell normal modes in "nonreciprocal" media which have broken time-reversal symmetry.

B. Frequency dependence of the dielectric medium

The formalism discussed so far treats the constitutive relations as static. In general, although we will treat them as spatially local, we cannot also treat them as instantaneous, and must in principle treat the local permittivity and permeability tensors as frequency dependent, $\boldsymbol{\epsilon}(\boldsymbol{r}) \to \boldsymbol{\epsilon}(\boldsymbol{r},\omega)$, $\boldsymbol{\mu}(\boldsymbol{r}) \to \boldsymbol{\mu}(\boldsymbol{r},\omega)$. This is because the nondissipative time-reversal-symmetry-breaking component of these tensors is both imaginary and antisymmetric (as opposed to real symmetric) *and* is an odd function of frequency, making frequency dependence inescapable in principle.

These effects can, on the one hand, be treated in a Hamiltonian formulation by adding extra local harmonic oscillator modes representing local polarization and magnetization degrees of freedom of the medium that couple to the electromagnetic fields. The full description of this is again a set of harmonic oscillator degrees of freedom described by equations of the form (16). On the other hand, with the assumption that we are treating the electromagnetic modes in a frequency range that is not resonant with any internal modes of the medium (i.e., in a frequency range where the loss-free condition is satisfied), we can eliminate the internal modes to yield a purely electromagnetic description, but with frequency-dependent constitutive relations.

The details are given in Appendix A, but the result can be simply stated. If all oscillator degrees of freedom are explicitly described, the eigenvalue problem for the normal modes has the structure (16), where B_{ij}^{-1} is positive definite and real symmetric. This guarantees that the eigenvalues ω_λ are real. However, the normal modes in some positive frequency range $\omega_1 < \omega < \omega_2$ can be treated by eliminating modes with natural frequencies outside that range, to give a matrix-eigenvalue-like problem of much smaller rank of the form

$$\sum_j A_{ij} u_{j\lambda}^{\pm} = \pm \omega_\lambda \sum_j B_{ij}^{-1}(\omega_\lambda) u_{j\lambda}^{\pm}, \tag{24}$$

where $B_{ij}(\omega)$ is now a frequency-dependent matrix with a Kramers-Kronig structure. The matrix $B_{ij}(\omega)$ is no longer in general real symmetric, but provided the eliminated modes are not resonant in the specified frequency range it instead is generically complex Hermitian. The "eigenvalue equation" is now a self-consistent equation:

$$\sum_j A_{ij} u_{j\lambda}^{\pm}(\omega) = \pm \omega_\lambda(\omega) \sum_j B_{ij}^{-1}(\omega) u_{j\lambda}^{\pm}(\omega). \tag{25}$$

This must be solved by varying ω until it coincides with an eigenvalue. Unfortunately, while $B_{ij}^{-1}(\omega)$ is Hermitian and nonsingular in the dissipationless frequency range $\omega_1 < \omega < \omega_2$, it is *not* necessarily positive definite, so *a priori* the eigenvalues $\omega_\lambda(\omega)$ are not guaranteed to be real, except for the fact that we know that these equations were derived from a standard frequency-independent eigenvalue problem which does have real eigenvalues. As shown in Appendix A, the Kramers-Kronig structure of $B_{ij}(\omega)$ reflects the stability of the underlying full oscillator system, giving the condition that a modified matrix

$$\tilde{B}_{ij}^{-1}(\omega) = \frac{d}{d\omega}[\omega B_{ij}^{-1}(\omega)] \tag{26}$$

is positive-definite Hermitian in the specified frequency range, which is sufficient to guarantee reality of the eigenvalues in that range. Furthermore, the quadratic expression for the energy of a normal mode solution is given in terms of $\tilde{B}_{ij}^{-1}(\omega_\lambda)$ rather than $B_{ij}^{-1}(\omega_\lambda)$, reflecting the fact that the total energy of the mode resides in both the explicitly retained degrees of freedom (the "electromagnetic fields") and those that have been "integrated out" (the nonresonant polarization and magnetization modes of the medium):

$$x_i(t) = B_{ij}^{-1}(\omega_\lambda) u_{j\lambda}^{+} e^{i\omega_\lambda t} + \text{c.c.}, \quad \omega_\lambda > 0, \tag{27}$$

$$H = \frac{1}{2} \sum_{ij} \tilde{B}_{ij}^{-1}(\omega_\lambda) (u_{i\lambda}^{+})^* u_{j\lambda}^{+}, \quad \frac{dH}{dt} = 0. \tag{28}$$

If the frequency dependence of the positive-definite Hermitian matrix $\tilde{B}_{ij}(\omega)$ is negligible in the range $\omega_1 < \omega < \omega_2$, so $\tilde{B}_{ij}(\omega) \approx \tilde{B}_{ij}(\omega_0)$, with $\omega_0 = (\omega_1 + \omega_2)/2$, one can replace $B_{ij}^{-1}(\omega)$ in (24) by the positive-definite frequency-independent Hermitian matrix $\tilde{B}_{ij}^{-1}(\omega_0)$. This in turn allows the eigenvalue problem to be transformed into the standard Hermitian eigenvalue problem

$$H_{ij} w_j^{(\lambda)} = \omega_\lambda w_i^{(\lambda)}, \quad (\boldsymbol{w}^{(\lambda)}, \boldsymbol{w}^{(\lambda')}) = \delta_{\lambda\lambda'}, \tag{29}$$

with scalar product

$$(\boldsymbol{w}, \boldsymbol{w}') \equiv \sum_j w_j^* w_j', \tag{30}$$

valid for positive ω_λ in the frequency range where $\tilde{B}_{ij}(\omega) \approx \tilde{B}_{ij}(\omega_0)$, with

$$H_{ij} = [\tilde{B}^{1/2}(\omega_0) A \tilde{B}^{1/2}(\omega_0)]_{ij}, \tag{31}$$

and

$$u_{i\lambda}^{+} \propto \sum_j \tilde{B}_{ij}^{1/2}(\omega_0) w_{j\lambda}. \tag{32}$$

This allows well-known Berry-curvature formulas from the standard Hermitian eigenproblem [5] to be quickly translated into the generalized problem. It turns out that, when the full problem with frequency-dependent constitutive relations is treated, the standard formula for the *Berry connection* remains correct with the simple replacement $\tilde{B}_{ij}(\omega_0) \to \tilde{B}_{ij}(\omega_\lambda)$ (the Berry curvature and Berry phase can both be expressed in terms of this Berry connection).

C. Berry curvature in Hermitian eigenproblems

Let $H_{ij}(\boldsymbol{g})$ be a family of complex Hermitian matrices defined on a manifold parametrized by a set $\boldsymbol{g}$ of independent coordinates g^μ, $\mu = 1, \ldots, D$. It is assumed that the matrix is generic, so its eigenvalues are all distinct; as is well known, three independent parameters must be "fine tuned" to produce an accidental degeneracy between a pair of eigenvalues. Thus, if the parametric variation of the Hermitian matrix is confined to a two-parameter submanifold, each eigenvalue $\omega_\lambda(\boldsymbol{g})$ will generically remain distinct. Under these circumstances, the corresponding eigenvector is fully defined by the eigenvalue equation and normalization condition, up to multiplication by a unimodular phase factor, which can vary on the manifold:

$$w_{\lambda i}(\boldsymbol{g}) \to e^{i\phi(\mathbf{g})} w_{\lambda i}(\boldsymbol{g}). \tag{33}$$

This is the well-known "U(1) gauge ambiguity" of the complex Hermitian eigenproblem. Associated with each eigenvector is a gauge field (vector potential in the parameter space), called the "Berry connection:"

$$\mathcal{A}_\mu^{(\lambda)}(\boldsymbol{g}) = -i(\boldsymbol{w}_\lambda(\boldsymbol{g}), \partial_\mu \boldsymbol{w}_\lambda(\boldsymbol{g})), \quad \partial_\mu \equiv \frac{\partial}{\partial g^\mu}. \tag{34}$$

This field on the manifold is gauge dependent, like the electromagnetic vector potential $\boldsymbol{A}(\boldsymbol{r})$, but its curvature (the Berry curvature), the analog of the magnetic flux density $\boldsymbol{B}(\boldsymbol{r}) = \boldsymbol{\nabla} \times \boldsymbol{A}(\boldsymbol{r})$, is gauge invariant and given by

$$\mathcal{F}_{\mu\nu}^{(\lambda)}(\boldsymbol{g}) = \partial_\mu \mathcal{A}_\nu^{(\lambda)}(\boldsymbol{g}) - \partial_\nu \mathcal{A}_\mu^{(\lambda)}(\boldsymbol{g}). \tag{35}$$

The Berry phase associated with a closed path Γ in parameter space is given (modulo 2π) by

$$\exp[-i\phi^{(\lambda)}(\Gamma)] = \exp\left(-i \oint_\Gamma \mathcal{A}_\mu(\boldsymbol{g}) dg^\mu\right). \tag{36}$$

Ignoring frequency dependence, the oscillator system has

$$\boldsymbol{H}(\boldsymbol{g}) = \boldsymbol{B}^{1/2}(\boldsymbol{g})\boldsymbol{A}\boldsymbol{B}^{1/2}(\boldsymbol{g}), \tag{37}$$

where the positive-definite Hermitian matrix $\boldsymbol{B}(\boldsymbol{g})$ can continuously vary as a function of some parameters $\boldsymbol{g}$, but $\boldsymbol{A}$ is invariant. Then conversion to the oscillator variables gives

$$\mathcal{A}_{\mu}^{(\lambda)}(\boldsymbol{g}) = \mathrm{Im}\left(\frac{(\boldsymbol{u}^{(\lambda)}, \tilde{\boldsymbol{B}}^{-1}(\boldsymbol{g}, \omega_{\lambda}) \partial_{\mu} \boldsymbol{u}^{(\lambda)})}{(\boldsymbol{u}^{(\lambda)}, \tilde{\boldsymbol{B}}^{-1}(\mathbf{g}, \omega_{\lambda}) \boldsymbol{u}^{(\lambda)})} \right). \tag{38}$$

Here $\boldsymbol{B}^{-1}(\boldsymbol{g})$ has been replaced by $\tilde{\boldsymbol{B}}^{-1}(\boldsymbol{g}, \omega_{\lambda})$ which is the correct result when the frequency dependence of $\boldsymbol{B}^{-1}(\boldsymbol{g}, \omega)$ is taken into account (see Appendix A).

D. Photonic bands and Berry curvature

In the case of periodic systems, the normal modes have discrete translational symmetry classified by a Bloch vector $\boldsymbol{k}$ defined in the Brillouin zone, i.e., defined modulo a reciprocal vector $\boldsymbol{g}$. For fixed $\boldsymbol{k}$, the spectrum of normal mode frequencies $\omega_n(\boldsymbol{k})$ is discrete, labeled by band indices n, and, as emphasized by Sundaram and Niu [4] in the electronic context, the Bloch vector of a wave packet plays the role of the control-parameter vector $\boldsymbol{g}$.

In order to compute the Berry curvature of the photon band Bloch states, we shall find it convenient to work in a fixed Hilbert space for all Bloch vectors $\boldsymbol{k}$, and we do this by performing a unitary transformation on the $\boldsymbol{A}$ matrix [which becomes the 6×6 matrix of differential operators (20) in the continuum formulation of the Maxwell equations] as

$$\boldsymbol{A}(\boldsymbol{k}, \boldsymbol{\nabla}) \equiv e^{-i\boldsymbol{k}\cdot\boldsymbol{r}} \boldsymbol{A}(\boldsymbol{\nabla}) e^{i\boldsymbol{k}\cdot\boldsymbol{r}} = \boldsymbol{A}(\boldsymbol{\nabla} + i\boldsymbol{k}). \tag{39}$$

Note that parametric dependence on the Bloch vector $\boldsymbol{k}$ is a little different from parametric dependence on parameters $\boldsymbol{g}$ that control the Hamiltonian. After projection into a subspace of fixed $\boldsymbol{k}$, the $\boldsymbol{A}$ matrix also becomes parameter dependent, while (if the constitutive relations are taken to be completely local) the $\boldsymbol{B}$ matrix in the photonics case is only implicitly $\boldsymbol{k}$ dependent through its self-consistent dependence on the frequency eigenvalue. [The parameter dependence of the $\boldsymbol{A}$ matrix does not affect the expression (38) for the Berry connection.]

The discrete eigenvalue spectrum $\omega_n(\boldsymbol{k})$ is then obtained by solving the self-consistent matrix-differential-equation eigenvalue problem

$$\boldsymbol{A}(\boldsymbol{k}, \boldsymbol{\nabla}) \boldsymbol{u}_n(\boldsymbol{k}, \boldsymbol{r}) = \omega_n(\boldsymbol{k}) \boldsymbol{B}^{-1}(\boldsymbol{r}, \omega_n(\boldsymbol{k})) \boldsymbol{u}_n(\boldsymbol{k}, \boldsymbol{r}), \tag{40}$$

where $\boldsymbol{B}^{-1}(\boldsymbol{r}, \omega)$ is the 6×6 block-diagonal permittivity-permeablity tensor $\mathrm{diag}(\boldsymbol{\epsilon}(\boldsymbol{r}, \omega), \boldsymbol{\mu}(\boldsymbol{r}, \omega))$, and $\boldsymbol{u}_n(\boldsymbol{k}, \boldsymbol{r}) \times \exp i\boldsymbol{k}\cdot\boldsymbol{r}$ represents the six-component complex vector $(\tilde{\boldsymbol{E}}_n(\boldsymbol{k}, \boldsymbol{r}), \tilde{\boldsymbol{H}}_n(\boldsymbol{k}, \boldsymbol{r}))$ of electromagnetic fields of the normal mode with Bloch vector $\boldsymbol{k}$ and frequency $\omega_n(\boldsymbol{k})$. The eigenfunction satisfies the periodic boundary condition $\boldsymbol{u}_n(\boldsymbol{k}, \boldsymbol{r} + \boldsymbol{R}) = \boldsymbol{u}_n(\boldsymbol{k}, \boldsymbol{r})$, where $\boldsymbol{R}$ is any lattice vector of the photonic crystal, and $\boldsymbol{B}^{-1}(\boldsymbol{r} + \boldsymbol{R}, \omega) = \boldsymbol{B}^{-1}(\boldsymbol{r}, \omega)$.

The transcription of Eq. (38) to the case of periodic media then gives the three-component Berry connection (vector potential) in $\boldsymbol{k}$ space as

$$\mathcal{A}_{(n)}^{a}(\boldsymbol{k}) = \mathrm{Im}\left(\frac{(\boldsymbol{u}_n(\boldsymbol{k}), \tilde{\boldsymbol{B}}^{-1}(\omega_n(\boldsymbol{k})) \boldsymbol{\nabla}_k^a \boldsymbol{u}_n(\boldsymbol{k}))}{(\boldsymbol{u}_n(\boldsymbol{k}), \tilde{\boldsymbol{B}}^{-1}(\omega_n(\boldsymbol{k})) \boldsymbol{u}_n(\boldsymbol{k}))} \right). \tag{41}$$

The scalar products in Eq. (41) are defined by the trace over the six components of $\boldsymbol{u}_n(\boldsymbol{k}, \boldsymbol{r})$, plus integration of the spatial coordinate $\boldsymbol{r}$ over a unit cell of the photonic crystal. By construction, if a Berry gauge transformation $\boldsymbol{u}_n(\boldsymbol{k}, \boldsymbol{r}) \rightarrow \boldsymbol{u}_n(\boldsymbol{k}, \boldsymbol{r}) \exp i\chi_n(\boldsymbol{k})$ is made, $\mathcal{A}_{(n)}^{a}(\boldsymbol{k}) \rightarrow \boldsymbol{\mathcal{A}}_{(n)}^{a}(\boldsymbol{k}) + \boldsymbol{\nabla}_k^a \chi_n(\boldsymbol{k})$.

In three-dimensional $\boldsymbol{k}$ space, the antisymmetric Berry curvature tensor $\mathcal{F}_{(n)}^{ab}(\boldsymbol{k}) = \boldsymbol{\nabla}_k^a \boldsymbol{\mathcal{A}}_{(n)}^{b}(\boldsymbol{k}) - \boldsymbol{\nabla}_k^b \mathcal{A}_{(n)}^{a}(\boldsymbol{k})$ can also be represented as the three-component "Berry flux density" $\Omega_a^{(n)}(\boldsymbol{k}) = \epsilon_{abc} \boldsymbol{\nabla}_k^b \mathcal{A}_{(n)}^{c}(\boldsymbol{k})$ (the $\boldsymbol{k}$ space curl of the Berry connection), to emphasize the duality between $\boldsymbol{r}$ space and $\boldsymbol{k}$ space, and the analogy between Berry flux in $\boldsymbol{k}$ space and magnetic flux in $\boldsymbol{r}$ space,

If a wave packet travels adiabatically (without interband transitions) through a region with slow spatial variation of the properties of the medium, so the photonic normal mode eigenvalue spectrum can be represented as a position-dependent dispersion relation $\omega_n(\boldsymbol{k}, \boldsymbol{r})$, the wave packet must be accelerated as its mean Bloch vector $\boldsymbol{k}$ slowly changes to keep its frequency constant. When translated into the language of photonics, the semiclassical electronic equations of motion then become the equations of ray optics:

$$\hat{n}^a \frac{dk_a}{dt} = -\hat{n}^a \boldsymbol{\nabla}_a \omega_n(\boldsymbol{k}, \boldsymbol{r}), \tag{42}$$

$$\frac{dr^a}{dt} = \boldsymbol{\nabla}_k^a \omega_n(\boldsymbol{k}, \boldsymbol{r}) + \mathcal{F}_n^{ab}(\boldsymbol{k}, \boldsymbol{r}) \frac{dk_b}{dt}, \tag{43}$$

where $\hat{n} \propto d\boldsymbol{r}/dt$ is parallel to the ray path, $\boldsymbol{\nabla}_a \equiv \partial/\partial r^a$ and $\boldsymbol{\nabla}_k^a \equiv \partial/\partial k_a$ (it is useful to use covariant and contravariant indices to distinguish components of spatial coordinates r^a from the dual Bloch vector components k_a). The Bloch-space Berry curvature $\mathcal{F}_n^{ab}(\boldsymbol{k}, \boldsymbol{r})$ controls the additional "anomalous velocity [19]" correction in (43) to the familiar group velocity of a wave packet $v_n^a(\boldsymbol{k}) = \boldsymbol{\nabla}_k^a \omega_n(\boldsymbol{k})$, which is active only when the wave packet is being accelerated by the inhomogeneity of the medium.

Before we conclude our general discussion on Berry curvature in photon band systems, we must state the constraints inversion and time-reversal symmetries place on the tensor $\mathcal{F}_n^{ab}(\boldsymbol{k})$. In what follows, we will use the Bloch state $\boldsymbol{w}_n$ defined in Eq. (32). If inversion symmetry (I) is present, the periodic part of the Bloch state $\boldsymbol{w}_n(\boldsymbol{k})$ has the following property: $\boldsymbol{w}_n(\boldsymbol{k}) = \boldsymbol{w}_n(-\boldsymbol{k})$ whereas if time-reversal symmetry (T) is present, $\boldsymbol{w}_n(\boldsymbol{k}) = \boldsymbol{w}_n^*(-\boldsymbol{k})$. If only ($I$) is present, it then follows that $\mathcal{F}_n^{ab}(\boldsymbol{k}) = \mathcal{F}_n^{ab}(-\boldsymbol{k})$, whereas if only ($T$) is present, $\mathcal{F}_n^{ab} = -\mathcal{F}_n^{ab}(-\boldsymbol{k})$. If *both* symmetries are present, then the Berry curvature is identically zero everywhere except at isolated points of accidental degeneracy, where it is not well defined. When $\mathcal{F}_n^{ab}$ is nonzero, the phases of the Bloch vectors cannot all be chosen to be real. These properties will be crucial when we consider the effects of various symmetry-breaking perturbations on the photon band structure.

E. Topological structure of the photon bands

The main consequence of having bands with nonzero Berry curvature field is that, if the path C is closed and encloses an entire Brillouin zone, the single-valuedness of the state $\boldsymbol{w}_n$ requires that

$$\exp\left(\oint \mathcal{A}_n^a dk_a\right) = \exp\left(\int\int dk_a \wedge dk_b \mathcal{F}_n^{ab}\right) = 1$$

or

$$\int\int_{S_C} dk_a \wedge dk_b \mathcal{F}_n^{ab} = 2\pi \mathcal{C}_n^{(1)}, \tag{44}$$

where $\mathcal{C}_n^{(1)}$ is an integer, known as the *Chern invariant* associated with the nth band, and have well-known consequences in the quantum Hall effect: in the integer quantum Hall effect, where the interactions among electrons are weak, the Hall conductance is expressed in terms of the sum of all Chern invariants of bands below the Fermi level [14]:

$$\sigma_H = \frac{e^2}{2\pi\hbar} \sum_{i,\epsilon_i<\epsilon_f} \mathcal{C}_i^{(1)}. \tag{45}$$

The gauge structure of the photon band problem outlined above is formally analogous to the local U(1) gauge invariance of ordinary electromagnetism. Note that the gauge invariance refers to the phase of the six-component electromagnetic fields as a whole; adding arbitrary phase $\boldsymbol{k}$-dependent phase factors to each field separately will in general not preserve the Maxwell equation constraint.

A phase convention can be specified, for instance, by arbitrarily choosing real and imaginary axes of the phases; the local gauge-dependent phase fields of the electromagnetic Bloch states are then represented as two-component rotor variables at each point of the Brillouin zone. In addition, a gauge choice may be made separately for each band so long as the spectrum remains nondegenerate [20,24].

By representing the phase covering on the Bloch manifold is this way, the possibility of the occurrence of topological defects of the gauge field becomes transparent. Local gauge transformations correspond to local smooth deformations of the rotor variables, and the Chern invariant corresponds to the total winding number of these rotor variables along a closed path enclosing the entire Brillouin zone.

In the case of two-dimensional Bloch bands, the defects of the phase field are point singularities, having a zero-dimensional "core" region where a phase convention is not well defined, due to quasidegeneracies with neighboring bands. It is clear that bands can have nonzero Chern numbers only if time-reversal symmetry is broken. Otherwise, the Berry curvature will be an odd function of k, and its integral over the entire 2D Brillouin zone vanishes (Fig. 1).

In three dimensions, the defects of the phase field are line defects or vortices and their stability requires quasidegeneracies to occur along isolated *lines* in reciprocal space.

In the photonic system of interest, even if photon bands can have nonzero Chern numbers, there can be no Hall conductance as given above due to their Bose statistics (and hence to their finite compressibility). However, the connection between *edge modes* and Chern invariants is independent of statistics: if the Chern number of a band changes at an interface, the net number of unidirectionally moving modes localized at the interface is given by the *difference* between the Chern numbers of the band at the interface (Fig. 2). We shall consider the problem of how Chern numbers can change across an interface in the next section.

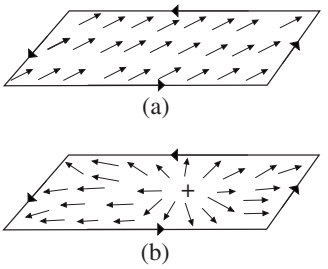

FIG. 1. A representation of the phase fields of the photonic Bloch states in a two-dimensional Brillouin zone using two component rotors. The entire set of six electric and magnetic fields is associated with a single phase at each point in the Brillouin zone. The Chern invariant simply represents the winding number of this phase along the Brillouin zone boundary and is also given by the integral of the Berry curvature $\mathcal{F}^{xy}$ over the two-dimensional Brillouin zone. The phases in (a) correspond to bands with both inversion and time-reversal symmetries, and the phases of the band can be chosen to be real everywhere in the Brillouin zone. For bands having nonzero Chern invariants (b), the phase around the zone boundary winds by an integer multiple of 2π and there is a phase-vortex-like singularity somewhere in the Brillouin zone where the Berry connection cannot be defined, due to the occurrence of quasidegeneracies.

Since the Chern invariant of a band is a topological number, it therefore cannot vary smoothly as we vary some parameter of the periodic eigenproblem. So long as a band remains nondegenerate, its Chern number cannot vary. However, if we tune some parameter λ of the Hamiltonian to a critical value λ_c such that two bands having nonzero Chern invariants touch at some isolated point in the Brillouin zone when $\lambda=\lambda_c$, the two bands can exchange their Chern numbers at these degenerate points (Fig. 3); if we tuned λ beyond its critical value, the bands will emerge with different Chern invariants. Since the total Berry "magnetic flux" of all bands remains fixed always, if only two isolated bands exchange their Chern numbers at points of degeneracy, the sum of their Chern numbers must remain invariant [5].

Generically, 2D bands with both time-reversal and inversion symmetry touch at isolated points of accidental degeneracy in a linear conical fashion, forming "Dirac cones" in the vicinity of which the spectrum is determined by a massless Dirac Hamiltonian,

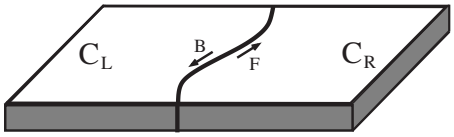

FIG. 2. The number of forward-minus the number of backward-moving edge modes equals the difference of the Chern number of the band across the interface.

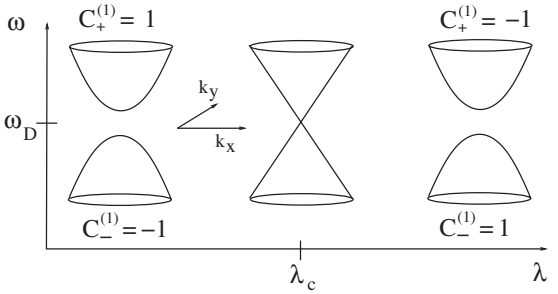

FIG. 3. As we tune some parameter λ of the Hamiltonian across a critical point where accidental degeneracies occur, and two bands touch in a linear fashion forming a Dirac point, Chern numbers of bands may be exchanged.

$$\mathcal{H} \equiv \omega - \omega_D = v_D(\delta k^1 \sigma_1 + \delta k^2 \sigma_2), \tag{46}$$

where v_D is a parameter that gives the slope of the cone close to the accidental degeneracy.

III. BROKEN *T* AND *I* IN PHOTONICS

In this section, we shall discuss our strategy for constructing photon bands with nonzero Chern invariants, and chiral edge states, whose existence is confirmed in the following sections.

To break time-reversal symmetry in photonics, we shall need magneto-optic materials (i.e., a Faraday-rotation effect). Such materials are characterized by their ability to rotate the plane of polarization of light, when placed in a magnetic field, and are used in conventional optical isolators. The amount of rotation per length is known as the Verdet coefficient, which depends on temperature as well as on the wavelength of light. Materials known to have large Verdet coefficients ($\sim 10^0$ mm^{-1} at wavelengths of the order of micrometers) are the iron garnet crystals such as $Ho_3Fe_50_{12}$ [21]. Due to the breaking of time-reversal symmetry in this materials, the eigenfrequency degeneracy is lifted for light characterized by different states of circular polarization.

While such magneto-optic devices employ magnetic fields in the direction of travel of the light beam, we shall be interested in two-dimensional photonic crystals with the magnetic fields placed perpendicular to the plane of propagation of light, as shown in Fig. 4. We shall call the axis perpendicular to the 2D photon bands the Faraday axis, and the setup here is reminiscent of a 2D electron gas (2DEG) placed in a perpendicular magnetic field.

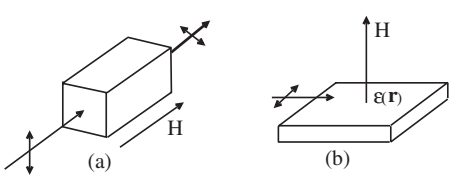

FIG. 4. In the conventional Faraday effect used in optical isolators (a), light travels in the same direction as the applied magnetic field, resulting in the rotation of its polarization plane. However, in the photonic analog of a 2DEG heterojunction proposed here (b), light travels in a direction perpendicular to the applied field.

Although we now have a means of introducing broken time-reversal symmetry, we still need a strategy for the nucleation of equal and opposite pairs of Chern invariants on bands near points of accidental degeneracy. To do this, we choose hexagonal lattice geometry. The threefold rotational symmetry of such a system guarantees the existence of Dirac points in the Brillouin zone corners when both inversion and time-reversal symmetry are *present*; in this case the only irreducible representations of the space group of threefold rotations correspond to nondegenerate singlets and degenerate doublets. As a simple example consider the case of free photon "bands" with dispersion $\omega = c|\boldsymbol{k}|$ in the first Brillouin zone of a triangular lattice. The eigenfrequencies of the photons are sixfold degenerate at the zone corners. Adding a weak periodic perturbation in the constitutive relations will lift the degeneracy and the bands will now either be nondegenerate or will form degenerate doublets, as demanded by the symmetry of the perturbation. Due to the sixfold rotation symmetry, the doublets are allowed to have a linear dispersion close to the zone corners and will be our Dirac points of interest, whereas the nondegenerate singlet bands disperse quadratically. We shall provide explicit examples of hexagonal photonic band structures having Dirac points in Sec. V.

While the existence of such Dirac points are virtually guaranteed in triangular lattice systems, their *stability* has little to do with lattice geometry. Such points are stable in two dimensions only because of the presence of time-reversal symmetry and inversion symmetry, when the eigenvalue problem is a real symmetric one: in this case it is possible to find accidental degeneracies by varying just two parameters, according to the Wigner–von Neumann theorem. Thus, if the perfect hexagonal geometry of the constitutive relations is slightly distorted, the Dirac points will simply move elsewhere in the two-dimensional Brillouin zone. Provided that such distortions are not too strong such that an axis of twofold rotations is introduced, in which case the linear dispersion characteristic of a Dirac point is no longer allowed, or if the distortion is so great that the Dirac points meet and annihilate at a point of inversion symmetry, Dirac points will still exist in the system.

If, however, inversion or time-reversal symmetry is broken in the system, the eigenvalue problem becomes complex Hermitian, and, according to the Wigner–von Neumann theorem, three parameters are required to ensure stability of the Dirac points—in this case, the Dirac point degeneracy of the 2D band structure is immediately lifted. In both cases, the two bands that split apart each acquire a nonzero Berry curvature field $\mathcal{F}_{xy}(\boldsymbol{k})$.

If inversion symmetry alone is broken, $\mathcal{F}_{xy}(\boldsymbol{k})$ is an *odd* function of $\boldsymbol{k}$, as discussed above. While the bands do have interesting semiclassical dynamics due to their anomalous velocity, they do not have any interesting topological properties since their Chern invariants are identically zero. On the other hand, if time-reversal symmetry alone is broken, via the Faraday coupling, the Berry curvature field will be an *even* function of $\boldsymbol{k}$, and each band which splits apart due to the Faraday coupling will have equal and opposite nonzero Chern invariants.

Finally, if we can slowly tune the Faraday coupling in *space*, from a positive value, across the critical value of zero,

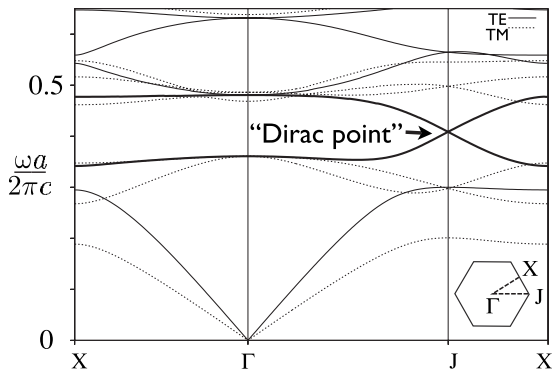

FIG. 5. Photon bands in the $k_z=0$ plane of a 2D hexagonal lattice of cylindrical dielectric rods. Electromagnetic waves are propagating only in the x-y plane (Brillouin zone shown in the lower right). As in Ref. [23], the rods have a filling fraction $f=0.431$, $\epsilon=14$, and the background has $\epsilon=1$. The band structure contains a pair of Dirac points at the zone corners (J).

where the local band-structure problem would permit Dirac spectra, to a negative value, we would generate a system of photonic bands with nonzero Chern numbers, that get exchanged at the region of space corresponding to the critical zero Faraday coupling. It then follows, that modes with exact correspondence to the integer-quantum-Hall edge states would arise in such a system. In the following section, we shall display this explicitly using an example band-structure.

IV. EXPLICIT REALIZATION OF EDGE MODES

An example of a photonic band structure with the desired properties is shown in Fig. 5. It consists of a triangular lattice of dielectric rods ($\epsilon_a=14$) placed in a background of air ($\epsilon=1$) with an area filling ratio of $f=0.431$. The authors of Ref. [23], in a quest for optimal photonic-band-gap materials, first studied this system. They computed the TE mode spectrum and found a full band gap in the TE spectrum. We have reproduced numerically their calculation and have also computed the spectrum for the TM modes.

The key feature of this particular system which is of importance to us is the presence of a pair of Dirac points in the spectrum of the TE modes which are well isolated from both the remaining TE and TM modes. Each of the six zone corners contains the Dirac cone spectrum, but there are only two distinct Dirac points, the others being related by reciprocal lattice translations of these points. In this particular system, the two Dirac points are related by inversion in $\boldsymbol{k}$ space.

As we have discussed, a gap immediately opens when either inversion or time-reversal symmetries are broken in this system. We break inversion symmetry in the simplest possible way by introducing a slight imbalance in the value of the dielectric tensor in the rods at opposite ends of the unit cell, and we parametrize the inversion breaking by defining the quantity

$$M_I = \ln\left(\frac{\epsilon_+}{\epsilon_-}\right), \tag{47}$$

where ϵ_+ (ϵ_-) is the value of the permittivity inside the rods in the upper (lower) half of the unit cell depicted in Fig. 5.

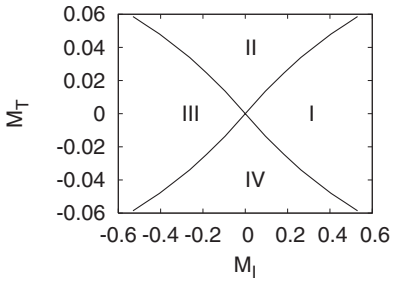

FIG. 6. Phase diagram of the photonic system as a function of inversion- and time-reversal-symmetry breaking. In regions I and III, the gap openings of both Dirac points are primarily due to inversion-symmetry breaking, whereas in regions II and IV, the breaking of time-reversal symmetry lifts the degeneracy of the bands that formed the Dirac point. In all four regions, the two bands of interest have nonzero Berry curvature, but only in regions II and IV do they contain nonzero Chern numbers.

To break time-reversal symmetry, we add a Faraday-effect term in the region outside the rods. This is done by giving the dielectric tensor a slight imaginary component without varying the constitutive relations inside the rods:

$$\epsilon_{ij}^{-1}(\boldsymbol{x}) = \begin{pmatrix} \epsilon_b^{-1} & i\Lambda \\ -i\Lambda & \epsilon_b^{-1} \end{pmatrix} \quad \text{(outside rods)}, \tag{48}$$

$$\epsilon_{ij}^{-1}(\boldsymbol{x}) = \begin{pmatrix} \epsilon_a^{-1} & 0 \\ 0 & \epsilon_a^{-1} \end{pmatrix} \quad \text{(inside rods)}. \tag{49}$$

We also define a parameter

$$M_T = \Lambda \tag{50}$$

to define the strength of the time-reversal-symmetry-breaking perturbation.

We first determined the phase diagram of the system in the (m_I, m_T) plane by breaking both inversion *and* time-reversal symmetry, and locating special values of the symmetry-breaking parameters that result in the closing of the band gap at one or more Dirac points (Fig. 6). The phase diagram separates regions characterized by bands just below the band gap having a nonzero Chern number from regions with all bands having zero Chern numbers. The boundaries between these phases are where the gap at one or more of the Dirac points vanishes, as shown in Fig. 6. Since there are two Dirac points, each phase boundary corresponds to the locus of parameters for which the gap at one of the Dirac points closes. Thus, both Dirac points close only when the two lines intersect, namely, at the point ($m_I=0$, $m_T=0$), where both inversion and time-reversal symmetries are simultaneously present. When inversion symmetry alone is broken, the Berry curvature field of Dirac point 1 is equal in magnitude and opposite in sign to the Berry curvature at the second Dirac point. When time-reversal symmetry is broken, on the other hand, each Dirac point has an identical (in both magnitude and sign) Berry curvature field. In this case, the photon bands which split apart at the Dirac point each have nonzero Chern number, which depends only on the direction of the Faraday axis ($\pm\hat{z}$).

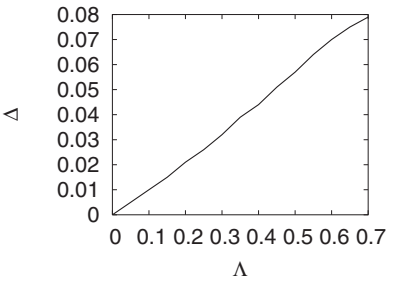

FIG. 7. The band gap (in units $\omega a/2\pi c$) opened by time-reversal-symmetry breaking as a function of the strength of the Faraday coupling Λ (same units as ϵ_b^{-1}) showing that the gap is linearly proportional to Λ.

We have also studied numerically the frequency gap as a function of the time-reversal-breaking perturbation above and found that, so long as the dielectric tensor remains positive definite, the gap increases linearly with ϵ_{xy} (Fig. 7). This will be important when we consider effective Dirac Hamiltonians for this problem: as we shall see, the fact that exactly at the zone corner the gap rises linearly with M_T is consistent with the spectrum of a massive Dirac Hamiltonian with mass M_T. Thus, we have shown an example of a band structure which contains Dirac points whose gaps can be tuned using time-reversal- and inversion-symmetry-breaking perturbations. We can now show the existence of chiral edge states in this system.

To study edge states in this system, we introduce a "domain wall" configuration across which the Faraday axis reverses. As we shall now show numerically (and justify analytically in the following section), the edge modes that occur along the domain wall are bound states that decay exponentially away from the wall while propagating freely in the direction parallel to the interface. In order to study the exponential decay of these modes, we glue together N copies of a single hexagonal unit cell along a single lattice translation direction $\boldsymbol{R}_\perp$, which will be the direction perpendicular to the domain wall. We treat this composite cell as a unit cell with periodic boundary conditions. Since a domain corresponds to a certain direction of the Faraday axis, we study a configuration here in which the axis changes direction abruptly across the domain wall from the $+\hat{z}$ to the $-\hat{z}$ direction.

When we consider the spectrum on a torus, there are necessarily two domain walls. Furthermore, since many unit cells are copied in this system, there are as many duplicates of the bands in the enlarged system under consideration. We study the band gap precisely at the Dirac point as a function of the fractional distance between the two domain walls on the torus x (Fig. 8) for a composite unit cell consisting of $N=30$ unit cells copied along the $\boldsymbol{R}_\perp$ direction. When $x=0$ or 1, the two domain walls are at the same point, and this corresponds to a single domain with a single Faraday coupling Λ. For all other values of x, the "unit cell" comprises a two-domain system with nonequivalent lengths. In Fig. 9, the gap between the two bands closest to the Dirac frequency decays exponentially as a function of the distance between the two domain walls. We shall show that the exponential decay in the gap corresponds to the localization of the edge modes along each domain wall. The small gap at intermediate values of x when the two walls are far apart corresponds to the fact that each edge mode has a small amplitude, and therefore hardly mix with each other at those length scales.

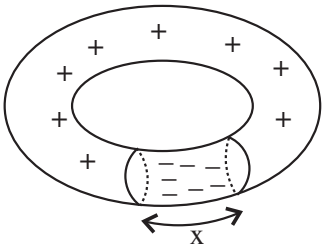

FIG. 8. In a system with periodic boundary conditions, there are necessarily two domain walls separating regions with different Faraday axes. We study the gap of the spectrum at the (now nondegenerate) Dirac points as a function of the distance $\boldsymbol{x}$ between the two walls.

When the domain wall is introduced, translational symmetry is still preserved along the direction parallel to the wall, and the states of the composite system of 30 unit cells can be labeled by $\boldsymbol{k}_\parallel$, the Bloch vectors in the direction parallel to the wall. Figures 10–12 consist of a spectral series of a system without any broken time-reversal symmetry (Fig. 10), with uniformly broken time-reversal symmetry (Fig. 11), and a domain wall configuration (Fig. 12) for the 30-unit-cell composite system. The bands are plotted along a trajectory in $\boldsymbol{k}$ space in the $\boldsymbol{k}_\parallel$ direction which contains the two distinct Brillouin zone corners. It is clear that in the domain wall there are two additional modes formed in the band gap that arose from the Faraday coupling. Since the domain walls are duplicated on the torus, the spectrum of edge modes will also be doubled; in Fig. 12, only the two nonequivalent modes are shown. Each mode in the band gap has a free photon linear dispersion along the direction of the wall; moreover, both have positive group velocities, and therefore propagate *unidirectionally*.

To be certain, however, that these chiral modes are indeed localized near the interface, we have numerically computed $\langle u(\boldsymbol{r})|\boldsymbol{B}^{-1}|u(\boldsymbol{r})\rangle$, the electromagnetic energy density (the $\boldsymbol{B}$ matrix, defined in Sec. II, is not to be confused with the magnetic flux density) or the photon probability density in

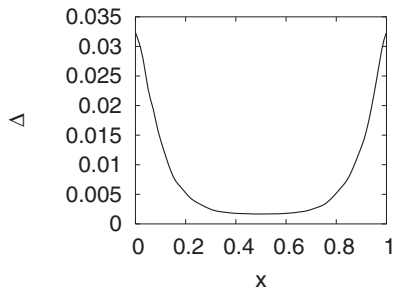

FIG. 9. The spectral gap (in units of $\omega a/2\pi c$) between the two bands which split apart due to the breaking of time-reversal symmetry. The spectrum is computed on a torus for the extended system consisting of 30 copies of the hexagonal unit cell. Furthermore, domain walls, across which the sign of the Faraday axis flips, are introduced, and the spectrum is plotted as a function of the separation $\boldsymbol{x}$ between the walls (see also Fig. 8).

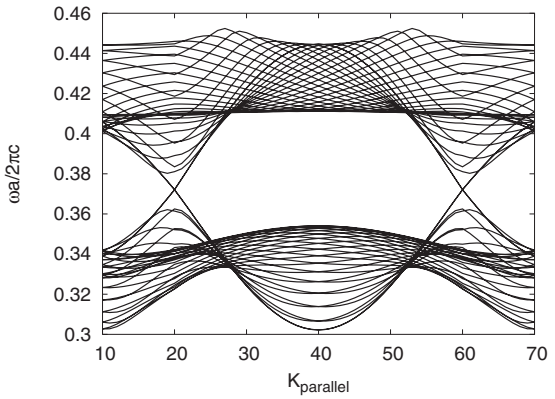

FIG. 10. The spectrum of the composite system consisting of 30 copies of a single hexagonal unit cell duplicated along the direction $\boldsymbol{R}_{\perp}$. Both inversion and time-reversal symmetries are present, and the Dirac points are clearly visible. While the composite system has a spectrum containing many bands, only two bands touch at the Dirac point. The dispersion is computed in $\boldsymbol{k}$ space along the direction *parallel* to the wall. The units of the horizontal axis are arbitrary: here we have discretized the points in $\boldsymbol{k}$ space along a line in the K_{parallel} direction which contains both Dirac points and present the photon spectrum at each point.

real space. We have computed this quantity along with all the spectra of the composite system using the real-space band-structure algorithms described in Appendix B. As shown in Fig. 13, the energy density is a Gaussian function, peaked at the position of the domain wall, and decaying exponentially away from the wall. From this calculation, we extract a localization also approximately five unit translations in the direction perpendicular to the interface.

We have therefore shown here using explicit numerical examples that photonic analogs of the chiral edge states of the integer quantum Hall effect can exist along domain walls of hexagonal photonic systems with broken time-reversal symmetry. We have studied the unphysical case in which such domain walls are abrupt changes in the axis of the Faraday coupling. However, due to the topological nature of these modes, a smoother domain wall in which the Faraday axis slowly reverses over a length scale much larger than a

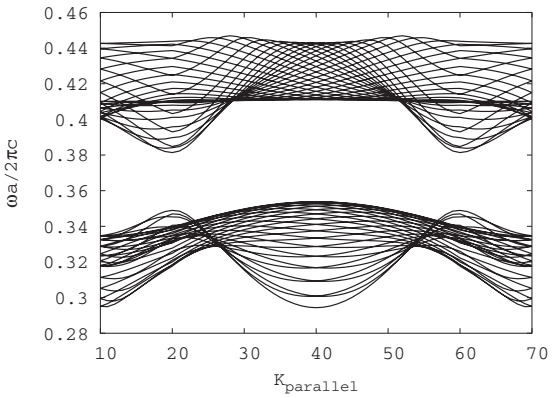

FIG. 11. The same system as above, but with broken time-reversal symmetry without a domain wall. There is a single Faraday axis in the rods of the entire system.

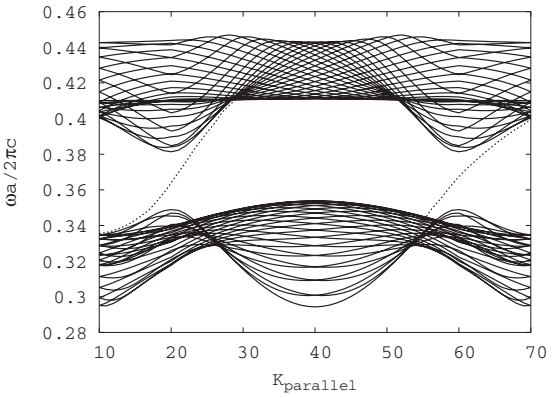

FIG. 12. Same system in Fig. 11, but with a domain wall introduced corresponding to maximum separation of the walls on the torus. The two additional modes present in the gap correspond to edge modes with a "free photon" linear dispersion along the wall. There are two modes, since across the domain wall the Chern number of the band just below the band gap changes by 2.

unit cell dimension would also produce such modes. The most important requirement for the existence of these modes is that at some spatial location the Faraday coupling is tuned across its critical value. How this particular tuning is effected is irrelevant. In the following section, after deriving the effective Hamiltonians for these modes, we shall consider a smoothly varying Faraday coupling, which corresponds to an exactly soluble system, and shall show the evolution of these modes as the smoothness of the Faraday coupling is varied toward the step function limit considered here.

V. MODEL HAMILTONIAN APPROACH

The crucial feature exploited in the previous sections was the possibility of tuning band gaps at Dirac points by adding time-reversal-symmetry-breaking perturbations. Before adding these perturbations, the linear conical spectra at these Dirac points are governed by two dimensional massless Dirac Hamiltonians, and time-reversal- or inversion-

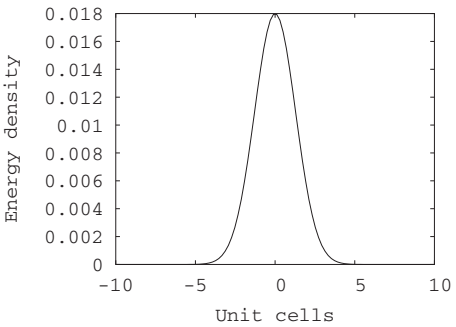

FIG. 13. The normalized real-space electromagnetic energy density profile associated with the edge modes in Fig. 12 plotted as a function of the direction *perpendicular* to the domain wall (and "integrated" over the direction parallel to the interface) and fitted to a Gaussian profile. The integrated energy density depicted here plays the role of the photon probability density, which confirms that light is confined to the interface.

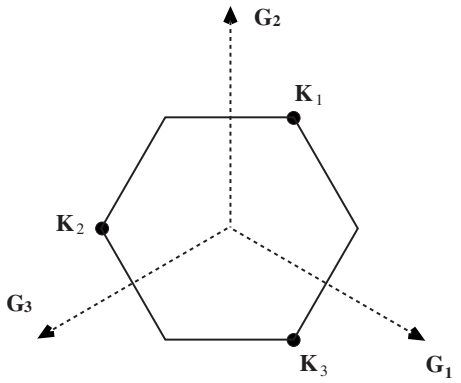

FIG. 14. In the weak-coupling approach, the free photon TE mode plane waves are perturbed by a periodic modulation in the permittivity. The plane wave frequency at the three equivalent zone corners ($\boldsymbol{K}_i$, $i=1,2,3$) is lifted by the permittivity in $\boldsymbol{k}\cdot\boldsymbol{p}$ perturbation theory into a nondegenerate singlet and a degenerate doublet.

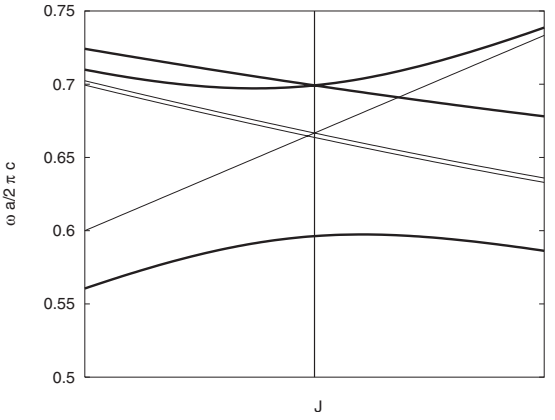

FIG. 15. Spectrum of photon dispersion in the vicinity of the zone corners. Here, the range of the horizontal axis is much smaller than a reciprocal lattice vector; we are showing the spectrum very close to the zone corner J where the nearly free approximation is valid. We have arbitrarily set $\lambda<0$ so that the singlet band has a lower frequency than the doublet. Free photon spectra are given by dashed lines. Away from the zone corners, the free spectrum is not affected to leading order in λ.

symmetry-breaking perturbations contribute *mass terms* to the Hamiltonian. In this section, we shall construct these Dirac Hamiltonians starting from the Maxwell equations for two-dimensional photonic systems with hexagonal symmetry.

To motivate Dirac Hamiltonians in photonic systems, we begin this section by considering a "nearly-free-photon" approach in which a two-dimensional free photon spectrum consisting of plane waves is perturbed by a weak periodic and hexagonal modulation of $\epsilon(\boldsymbol{r})$. Due to the underlying symmetry of the perturbation, the plane waves mix in such a manner as to generate Dirac points in the zone corners of this system. We then consider the effect of adding time-reversal- and inversion-symmetry-breaking perturbations in this system and derive an expression for the Dirac mass. Having motivated the Dirac points, we revert to our photon band problem and derive expressions for the Dirac mass in these systems.

In analogy with the nearly-free-electron approximation, we consider the photon propagation problem in the weak-coupling regime, in which the dielectric properties of the medium act as a weak perturbation. We solve the Maxwell normal mode problem for Bloch state solutions, and work out corrections to the free photon dispersion relations in the Brillouin zone boundaries. We shall assume continuous translational invariance in the z direction, and study the propagation of electromagnetic waves in the x-y plane.

The free photon constitutive relations are isotropic and uniform in the plane:

$$B_0 = \begin{pmatrix} \epsilon_0 & 0 \\ 0 & \mu_0 \end{pmatrix}. \tag{51}$$

We consider the free photon bands in the first hexagonal Brillouin zone depicted in Fig. 14. Let $\boldsymbol{G}_i$, $i=1,2,3$, be the three equal-length reciprocal lattice vectors each rotated 120° with respect to one another. The hexagonal zone corners correspond to the points $\pm\boldsymbol{K}_i$, where $\boldsymbol{K}_1=(\boldsymbol{G}_2-\boldsymbol{G}_3)/3$, etc., and $|\boldsymbol{K}|=|G|/\sqrt{3}$. At each of the zone corners, the free photon spectrum is sixfold degenerate with $\omega_0=c_0K$. In two dimensions, the modes decouple into TE (E_x,E_y,H_z) and TM (H_x,H_y,E_z) sets, and we shall focus only on the TE modes and consider the threefold TE mode symmetry at the zone corners (the TE and TM modes do not mix in two dimensions). The eigenvalue equation for the free photon plane wave modes at the zone corners is $\boldsymbol{A}|\boldsymbol{u}_0\rangle=\omega_0\boldsymbol{B}_0^{-1}|\boldsymbol{u}_0\rangle$, or equivalently $\boldsymbol{B}_0^{1/2}\boldsymbol{A}\boldsymbol{B}_0^{1/2}|z_0\rangle=\omega_0|z_0\rangle$ and the states $|z_0\rangle=\boldsymbol{B}_0^{-1/2}|\boldsymbol{u}_0\rangle$ satisfy $\langle z_0^{(\lambda)}|z_0^{(\lambda')}\rangle=\delta_{\lambda\lambda'}$.

Next, keeping the uniform isotropic permeability fixed, we add a weak periodic perturbation to the permittivity of the form

$$\lambda B_1^{-1} = \begin{pmatrix} \epsilon_0\lambda V_G(\boldsymbol{r}) & 0 \\ 0 & 0 \end{pmatrix} \tag{52}$$

with

$$V_G(\boldsymbol{r}) = 2\sum_{n=1}^{3} \cos(\boldsymbol{G}_n\cdot\boldsymbol{r}). \tag{53}$$

After this perturbation is added, the TE and TM modes no longer remain degenerate; while the TM modes remain threefold degenerate at the zone corners at the frequency $\omega=c_0|\boldsymbol{K}|$, the TE modes split apart into a singlet and a degenerate doublet as shown in Fig. 15. We now determine the splitting to leading order in λ within a weak-coupling nearly-free-photon approach.

With the periodic perturbation, the eigenvalue problem is

$$\boldsymbol{A}|\boldsymbol{u}\rangle = \omega(\boldsymbol{B}_0^{-1}+\lambda\boldsymbol{B}_1^{-1})|\boldsymbol{u}\rangle \tag{54}$$

which is equivalent to

$$\boldsymbol{B}_0^{1/2}(\boldsymbol{A}-\lambda\omega\boldsymbol{B}_1^{-1})\boldsymbol{B}_0^{1/2}|z\rangle = (\omega_0+\delta\omega)|z\rangle. \tag{55}$$

The energy splittings are worked out in degenerate perturbation theory (see Appendix C) as

$$\frac{\delta\omega_n}{\omega_0} = -\lambda\langle\tilde{z}_n|\boldsymbol{B}_0^{1/2}\boldsymbol{B}_1^{-1}\boldsymbol{B}_0^{1/2}|\tilde{z}_n\rangle = -\lambda\langle\tilde{\boldsymbol{u}}_n|\boldsymbol{B}_1^{-1}|\tilde{\boldsymbol{u}}_n\rangle,$$

where $|\tilde{z}_n\rangle$ are appropriate combinations of the three free photon plane-plane waves that diagonalize the periodic potential. These states are obtained by requiring them to be invariant under threefold rotations in the plane. Instead of writing the fields in the coordinate basis, it is convenient to use a redundant basis of the three vectors $(e^{i\boldsymbol{K}_1\cdot\boldsymbol{r}}, e^{i\boldsymbol{K}_2\cdot\boldsymbol{r}}, e^{i\boldsymbol{K}_3\cdot\boldsymbol{r}})$, with $\Sigma_n\boldsymbol{K}_n=\boldsymbol{0}$, and $\boldsymbol{K}_i\cdot\boldsymbol{K}_j=-K^2/2$, $i\neq j$. In this basis, the magnetic field of the TE modes is written as ($\eta=e^{2\pi i/3}$)

$$H_1^z = (1,1,1), \tag{56}$$

$$H_2^z = (1,\eta^*,\eta), \tag{57}$$

and

$$H_3^z = (1,\eta,\eta^*). \tag{58}$$

The corresponding electric flux densities are easily obtained:

$$D_1^{\parallel} = \frac{1}{\omega}(\hat{z}\times\boldsymbol{K}_1,\hat{z}\times\boldsymbol{K}_2,\hat{z}\times\boldsymbol{K}_3), \tag{59}$$

$$D_2^{\parallel} = \frac{1}{\omega}(\hat{z}\times\boldsymbol{K}_1,\eta^*\hat{z}\times\boldsymbol{K}_2,\eta\hat{z}\times\boldsymbol{K}_3), \tag{60}$$

$$D_3^{\parallel} = \frac{1}{\omega}(\hat{z}\times\boldsymbol{K}_1,\eta\hat{z}\times\boldsymbol{K}_2,\eta^*\hat{z}\times\boldsymbol{K}_3), \tag{61}$$

and

$$|\tilde{z}_i\rangle = \begin{pmatrix} E_i^{\parallel} \\ H_i^z \end{pmatrix}. \tag{62}$$

Clearly, these are the plane wave solutions that satisfy Maxwell equations and transform appropriately under threefold rotations in the plane. We are therefore led to the simple result that the splitting at the zone corners due to the mixing of the three plane waves is related to the integral over the unit cell of the electric fields and the periodic potential, which is a traceless, real symmetric 3×3 problem. It is easy to see that the problem is traceless because diagonal terms of the form $\langle u_i|B_1|u_i\rangle$ vanish identically since u_i are plane waves.

To leading order in λ, the three photon bands split to form a singlet band at frequency $\omega_0=c_0|K|[1+\lambda/2+O(\lambda^2)]$ and a degenerate doublet at frequency

$$\omega_D = c_0|K|[1-\lambda/4+O(\lambda^2)]. \tag{63}$$

Exactly at the zone corners, the singlet and doublet states above diagonalize the perturbation in Eq. (52). To leading order in λ and $\delta\boldsymbol{k}\equiv\boldsymbol{k}-\boldsymbol{K}_i$, the deviation in the Bloch vector from the zone corners, the states $|\tilde{z}_2(\delta\boldsymbol{k})\rangle$ and $|\tilde{z}_3(\delta\boldsymbol{k})\rangle$ [where $|\tilde{z}_i(\delta\boldsymbol{k})\rangle=\exp(i\delta\boldsymbol{k}\cdot\boldsymbol{r})|\tilde{z}_i\rangle$], which are degenerate at $\delta\boldsymbol{k}=\boldsymbol{0}$, mix and split apart linearly as a function of $|\delta\boldsymbol{k}|$, forming a Dirac point. To leading order, the Dirac point doublet does not mix with the singlet state $|\tilde{z}_1(\delta\boldsymbol{k})\rangle$. The effective Hamiltonian governing the spectrum of the doublet, to leading order in $\delta\boldsymbol{k}$, is a 2D massless Dirac equation:

$$\omega_{\pm}(\delta\boldsymbol{k}) = \omega_D \pm v_D(\delta k_x\sigma^x + \delta k_y\sigma^y), \tag{64}$$

where $v_D=c_0/2+O(\lambda)$, and σ^i are the Pauli matrices written in the subspace of the doublet states. The linear dispersion of the doublet in the neighborhood of the zone corners is immediately obtained by solving Eq. (64):

$$\omega = \omega_D \pm v_D|\delta\boldsymbol{k}|. \tag{65}$$

The singlet band's frequency remains unchanged to leading order in $\delta\boldsymbol{k}$: $\omega_0(\delta\boldsymbol{k})=\omega_0+O(|\delta\boldsymbol{k}|^2)$. Thus, we have shown that the periodic modulation of the permittivity having threefold rotational symmetry gives rise to a quadratically dispersing singlet band and a Dirac point with linear dispersion.

Next, we add a Faraday term, with its axis normal to the xy plane, to the permittivity tensor $\epsilon^{xy}=-\epsilon^{yx}=i\epsilon_0\eta(\boldsymbol{r},\omega)$, where

$$\eta(\boldsymbol{r},\omega) = \eta_0(\omega) + \eta_1(\omega)V_G(\boldsymbol{r}). \tag{66}$$

Both $\eta_0(\omega)$ and $\eta_1(\omega)$ are odd functions of ω. In the limit that the Faraday coupling is much weaker in strength than the periodic modulation, $|\eta_0|,|\eta_1|\ll|\lambda|\ll1$, the mixing between the nondegenerate singlet state and the doublet remains negligible, and the energy of the singlet state is unaffected by the Faraday perturbation. However, the doublet states split apart at the Dirac point. Using the expression for the Dirac point splitting, derived in Appendix C, we find that the splitting of the doublet at the zone corner is given by

$$\omega_{\pm}-\omega_D = \pm v_D\kappa, \kappa = |K|\left(\frac{3}{2}\eta_1(\omega_D) - 3\lambda\,\eta_0(\omega_D)\right). \tag{67}$$

Away from the Dirac point (but still close enough to the zone corners so that the nearly-free-photon approximation for the three plane wave states remains valid), the doublet bands acquire a dispersion

$$\omega = \omega_D \pm v_D(|\delta\boldsymbol{k}|^2+\kappa^2)^{1/2}, \tag{68}$$

which is the spectrum of a 2D massive Dirac Hamiltonian:

$$\omega_{\pm}(\delta\boldsymbol{k}) = \omega_D \pm v_D(\delta k_x\sigma^x + \delta k_y\sigma^y + \kappa\sigma^z). \tag{69}$$

The Dirac points that occur in the nearly-free-photon approximation are not isolated points of degeneracy, since, away from the zone corners, the two bands which formed the Dirac point merge together to resume their original free photon form. Consequently, the type of modes studied in the previous section cannot be reproduced using this type of weak-coupling expansion.

However, we can gain understanding by supposing that we have the exact solutions of the electromagnetic Bloch states and eigenfrequencies of a system containing isolated Dirac points, such as the one studied numerically in Sec. IV. We can use precisely the same weak-Faraday-coupling approximation to work out the splitting of the Dirac point with a Faraday term. Assuming we are given example photonic band structures of long hexagonal systems with $k_z=0$, which contain only isolated Dirac points, a weak Faraday coupling will split apart the bands that formed the Dirac point, and the splitting is identical to that in (68). Suppose that the two

bands having a Dirac point otherwise form a PBG with a gap $\Delta \gg v_D\kappa$ (as in the case of the numerical example given in the previous section). In this case, since the Faraday term removes all points of degeneracy, the now nondegenerate bands have a well-defined Berry curvature field

$$\mathcal{F}_{\pm}(\delta\boldsymbol{k}) = \pm \frac{1}{2}\kappa(|\delta\boldsymbol{k}|^2 + \kappa^2)^{-3/2}, \tag{70}$$

which decays rapidly away from the Dirac point, and contributes a total integrated Berry curvature of $\pm\pi$. Since there are two nonequivalent Dirac points in the hexagonal geometry under consideration, the net Berry curvature of the system is the sum of the contributions from each Dirac point. If, as in the case under consideration, spatial inversion symmetry is preserved but time-reversal symmetry is broken, the Berry curvature fields at each Dirac point of a given band add, giving total Chern numbers ± 1 for each of the split bands. However, if time-reversal symmetry is preserved, and inversion-symmetry breaking causes the gap to open, the Berry curvature fields of each Dirac point for a given band are equal in magnitude but opposite in sign, and the Chern number vanishes.

As before, to get unidirectional edge modes of light in this system, the Faraday coupling must be tuned across its critical value $\eta(\boldsymbol{r},\omega)=0$. To do this, we consider a Faraday coupling that varies slowly and adiabatically in space, we assume negligible frequency dependence of the Faraday coupling, and we parametrize the local value of the Faraday coupling by a smoothly varying function $\kappa(\boldsymbol{r})$, which is positive in some regions and negative in other regions of the 2D plane perpendicular to the cylindrical axis of the hexagonal array of rods. Due to the adiabatic variation of $\kappa(\boldsymbol{r})$, each point in space is characterized by a local band-structure problem, and the splitting at the Dirac point is given again by the expression in (68), but with the local value of κ. In this limit, the smooth variation of $\kappa(\boldsymbol{r})$ leads to a 2D Dirac Hamiltonian with an adiabatically spatially varying mass gap. At all points where $\kappa(\boldsymbol{r})=0$, the local band structure in the vicinity of the Dirac point is the massless 2D Dirac Hamiltonian; provided that $|\kappa(\boldsymbol{r})| \ll \Delta$, the PBG, the spectrum far away from the Dirac points is unaffected by $\kappa(\boldsymbol{r})$. In what follows, we assume that, when $\kappa=0$, our band structure contains Dirac points which are formed by two isolated bands in a PBG region having no other points of degeneracy.

We neglect the mixing between modes at different Dirac points, and consider the situation in which $\kappa(\boldsymbol{r})$ vanishes along a single line ($x=0$ for instance), and we assume translational invariance along the direction parallel to the interface (y direction). As before, we consider the degenerate perturbation problem of the normal modes close to the Dirac point. Now, however, the coefficients of the degenerate solutions of the Maxwell equations are spatially varying quantities. Let $|u_\sigma(\pm\boldsymbol{k}_D)\rangle$, $\sigma=\pm$, be the degenerate solutions (i.e., the periodic parts of the photon Bloch state wave functions) at a pair of Dirac points when $\kappa=0$. With the local variation, we take a spatially varying linear combination of these Bloch states,

$$u(\boldsymbol{k}_D,\boldsymbol{r}) = \sum_{\sigma,\pm} \psi_\sigma(\boldsymbol{r})\exp(\pm i\boldsymbol{k}_D\cdot\boldsymbol{r})u_\sigma(\pm\boldsymbol{k}_D,\boldsymbol{r}), \tag{71}$$

and arrive at the fact that the local value of the splitting of the two bands at $\boldsymbol{k}_D$ is

$$\omega_+(\boldsymbol{k}_D) - \omega_-(\boldsymbol{k}_D) = 2\kappa(\boldsymbol{r}). \tag{72}$$

In the neighborhood of the Dirac point, the degenerate perturbation problem gives us a 2D massive Dirac Hamiltonian, with δk_x replaced by the operator $-i\boldsymbol{\nabla}_x$ in the position representation, since translation symmetry in the x direction is broken by $\kappa(x)$. We thus obtain an expression of the form $v_D\hat{K}|\psi\rangle = \delta\omega|\psi\rangle$, and

$$\hat{K} = -i\boldsymbol{\sigma}^x\boldsymbol{\nabla}_x + \delta k_\parallel\boldsymbol{\sigma}^y + \kappa(x)\boldsymbol{\sigma}^z. \tag{73}$$

The Bloch vector in the y direction, which remains conserved due to the preservation of translation invariance along this direction, is $k_{Dy}+\delta k_\parallel$.

For the particular choice of $\kappa(x)=\kappa^\infty \tanh(x/\xi)$, $\xi>0$ (where κ^∞ is the asymptotic value of the Dirac point splitting at distances $\gg\xi$ from the interface), the problem is exactly solvable, since the Dirac Hamiltonian $\hat{K}$, when squared, becomes a 1D Schrödinger Hamiltonian $\hat{K}^2$ corresponding to the integrable Pöschl-Teller Hamiltonian [22].

To see how this comes about, we explicitly work out the operator $\hat{K}^2$, making use of the anticommuting property of the Pauli matrices $\{\sigma^a,\sigma^b\}=2\delta^{ab}$:

$$\hat{K}^2 - \delta k_\parallel^2 = -\nabla_x^2 + \kappa(x)^2 - \boldsymbol{\sigma}^y\kappa'. \tag{74}$$

The spatially varying Dirac mass term that changed sign across the interface becomes a "potential well" with bound states given by [22]

$$\omega_0(\delta k_\parallel) = \omega_D + s_\kappa v_D\delta k_\parallel, \quad s_\kappa = \mathrm{sgn}(\kappa^\infty)$$

$$\omega_{n\pm} = \omega_D \pm v_D(\delta k_\parallel^2 + \kappa_n^2)^{1/2}, \quad n>0, \tag{75}$$

where $|\kappa_n| = 2n|\kappa^\infty|/\xi$, $n < |\kappa^\infty|\xi/2$. Figure 16 shows the normal mode spectrum of the Pöschl-Teller model. In the $n=0$ mode, light propagates *unidirectionally*, with velocity v_D, in the direction parallel to the wall. All other bound modes are bidirectional modes. The numerical example of a Dirac mass studied in the previous section that changed sign abruptly, as a step function, has the 1D Schrödinger problem in an attractive δ function potential as its square. Consequently, as we have seen, the model permitted only a single bound state, corresponding to the unidirectional mode.

For the generic case, the second-order differential equation for the $n>0$ bound states cannot be solved analytically. However, a formal solution for the zero-mode eigenfrequency can be obtained, as it is obtained by solving a *first-order* equation, as we now discuss. Starting from the Dirac equation for the more general case

$$v_D(-i\boldsymbol{\sigma}^x\boldsymbol{\nabla}_x + -i\boldsymbol{\sigma}^y\boldsymbol{\nabla}^y + \kappa(x)\boldsymbol{\sigma}^z)|\psi_\pm\rangle = \delta\omega|\psi_\pm\rangle, \tag{76}$$

by definition, the "zero mode" has free photon dispersion along the direction parallel to the wall, which implies that the function $|\psi\rangle \propto \exp(i\delta k_\parallel y)$. We are thus left with the equation

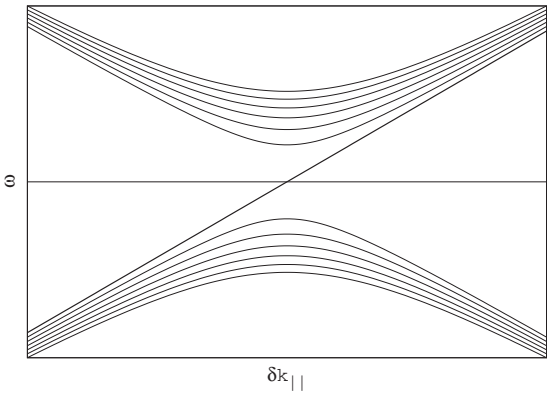

FIG. 16. Spectrum of the integrable Pöschl-Teller model, Eq. (75). The horizontal line corresponds to $\omega=\omega_D$. $\delta k_\parallel=0$ when the zero-energy mode crosses this line. At $\delta k_\parallel=0$, the first excited state has a frequency $\omega=2v_D|\kappa^\infty|/\xi$ and corresponds to bidirectional propagation. With the exception of the zero mode, all bound states correspond to bidirectionally propagating modes localized at the interface where the function $\kappa(\boldsymbol{r})=0$. The zero mode, on the other hand, is unbalanced, and furthermore it corresponds to unidirectional propagation.

$$[-i\boldsymbol{\sigma}^x\boldsymbol{\nabla}_x+\kappa(x)\boldsymbol{\sigma}^z]|\psi_\pm\rangle=0. \tag{77}$$

Multiplying both sides with $\boldsymbol{\sigma}^x$, we arrive at the following first-order differential equation:

$$(\boldsymbol{\nabla}_x+\kappa(x)\boldsymbol{\sigma}^y)=0, \tag{78}$$

which has as its formal solution

$$|\psi_\pm\rangle=\exp\left(i\delta k_\parallel y+\alpha\int^x dx'\,\kappa(x')\right)|\phi_\pm(\alpha)\rangle, \tag{79}$$

where $\boldsymbol{\sigma}^y|\phi_\pm(\alpha)\rangle=\alpha|\phi_\pm(\alpha)\rangle$. Although there are formally two solutions for the zero mode, corresponding to $\alpha=\pm1$, only one can occur; the other is not normalizable and thus cannot represent a physically observable state.

VI. SEMICLASSICAL ANALYSIS

Now let the Dirac mass term that opens the photonic band gap be a slowly varying function $\kappa(x)$ that changes monotonically (and analytically) from $-k_0$ at $x=-\infty$ to k_0 at $x=+\infty$. The photonic spectrum of modes with wave numbers $\boldsymbol{k}=\boldsymbol{k}_D+\delta\boldsymbol{k}$ near the Dirac point $\boldsymbol{k}_D$, and which become doubly degenerate at $\boldsymbol{k}_D$, is an adiabatic function of x:

$$\omega(x,\delta k_x,\delta k_y)=\omega_D\pm v_D[\delta k_y^2+k(x,\delta k_x)^2]^{1/2},$$

$$k(x,\delta k_x)^2=\delta k_x^2+\kappa(x)^2, \tag{80}$$

where $v_D>0$ is the Dirac speed. For $k(x,\delta k_x)^2<k_0^2$, the modes are evanescent as $x\to\pm\infty$ and so are localized on the wall. In the x-δk_x plane, the contours of constant $k(x,\delta k_x)^2<k_0^2$ are simple closed curves, enclosing a finite dimensionless area $\phi(k^2)$, given by

$$\phi(k^2)=2\int_{x_-}^{x_+}dx[k^2-\kappa(x)^2]^{1/2}, \tag{81}$$

where $x_-(k^2)<x_+(k^2)$ are the two "turning point" solutions of $\kappa(x_\pm)^2=k^2$. Since $\kappa(x)$ is assumed to be monotonic, this can be written as

$$\phi(k^2)=2\int_0^{|k|}dy(k^2-y^2)^{1/2}\left(\frac{1}{\kappa'_+(y^2)}+\frac{1}{\kappa'_-(y^2)}\right),$$

$$\kappa'_\pm(k^2)\equiv\left.\frac{d\kappa}{dx}\right|_{x_\pm(k^2)}. \tag{82}$$

Note that this transformation has turned $\phi(k^2)$ into a *signed* area, where $\mathrm{sgn}(\phi)=\mathrm{sgn}(k_0)$, which is indeed the correct form [the function $\phi(k^2)$ vanishes as $k_0\to0$, when its domain $k^2\leqslant k_0^2$ shrinks to zero]. In the limit $k^2\to0$, $x_\pm(k^2)\to x_0$, the formal location of the interface. Then $\kappa'_\pm(k^2)\to\kappa'(x_0)$, and $\phi(k^2)$ vanishes as

$$\phi(k^2)\to\frac{\pi k^2}{\kappa'(x_0)},\quad (k/k_0)^2\to0. \tag{83}$$

It is very instructive to examine the special case

$$\kappa(x)=k_0\tanh[\alpha(x-x_0)], \tag{84}$$

which is integrable. In this case,

$$\kappa'(x)=\alpha k_0\,\mathrm{sech}^2[\alpha(x-x_0)], \tag{85}$$

$$k_0\,\mathrm{sech}^2\{\alpha[x_\pm(k^2)-x_0]\}=\frac{k_0^2-k^2}{k_0}. \tag{86}$$

Thus the explicit dependence on $x_\pm(k^2)$ can be eliminated, and

$$\kappa'_\pm(k^2)=\alpha\left(\frac{k_0^2-k^2}{k_0}\right). \tag{87}$$

This make the integral for $\phi(k^2)$ trivial (it becomes expressible in terms of a simple Hilbert transform), and the asymptotic small-k^2 form (83) remains valid for *all* values of k^2 in the domain of the function

$$\phi(k^2)=\frac{\pi k^2}{\alpha k_0},\quad k^2\leqslant k_0^2. \tag{88}$$

Then the frequency of the interface mode with wave number $\delta k_y=\delta k_\parallel$ along the interface can be expressed as

$$\omega(\delta k_\parallel,\phi)=\omega_D\pm v_D[\delta k_\parallel^2+\kappa_\perp^2(\phi)]^{1/2},$$

$$\kappa_\perp^2(\phi)\equiv|\alpha k_0\phi|/\pi. \tag{89}$$

A standard semiclassical analysis of interference effects on a light ray trapped in a waveguide at an interface would conclude that the quantized values of ϕ corresponding to interface modes were

$$\phi_n=2\pi n+\gamma, \tag{90}$$

where γ is a Maslov phase, usually π. In this case, comparison with the exact solution of the integrable problem con-

firms that this problem instead has a vanishing Maslov phase $\gamma=0$. This can be attributed to an underlying Z_2 Berry phase factor of -1 (Berry phase of π) for orbiting around the degeneracy point at $(x-x_0,k_x)=(0,0)$.

We then conclude that the interface modes at a slowly varying interface are in general given (for small $\delta k_\parallel$) by

$$\omega_0(\delta k_\parallel) = \omega_D + v_D \,\mathrm{sgn}(\mathrm{k}_0)\delta k_\parallel,$$

$$\omega_{n\pm}(\delta k_\parallel) = \omega_D \pm v_D(\delta k_\parallel^2 + k_n^2)^{1/2}, \quad n \geqslant 1,$$

$$\phi(k_n^2) = 2\pi n, \quad k_n^2 \leqslant k_0^2. \tag{91}$$

The unidirectional zero mode persists, however sharp the interface is; the bidirectional modes with $n \geqslant 1$ must obey $2\pi n < \phi(k_0^2)$, which has fewer and fewer (and eventually no) solutions as the width of the interface region shrinks. In the special case of the integrable model (84), this spectrum is exact for small $\delta k_\parallel$ without any condition that the wall is slowly varying.

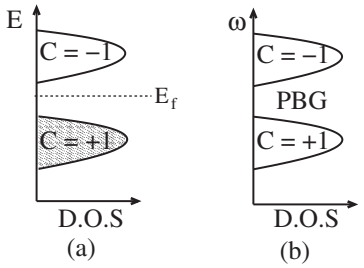

FIG. 17. Although the photon bands (b) cannot be filled as in the electronic case (a), they can have no analog of the bulk quantum Hall effect. However, the Chern number is a topological invariant of Bloch states independent of the constituents. With the Faraday term, we are able to tune the system such that the total Chern number below a photonic band gap changes across the interface, which gives rise to unidirectionally propagating edge modes of photons localized at the interface. These modes are direct analogues of the chiral edge modes of electronic systems which occur at interfaces between two regions having different total Chern invariants below the Fermi level (i.e., with different Hall conductances).

VII. DISCUSSION

The occurrence of zero-energy modes in the 2D Dirac Hamiltonian is well known and represents the simplest example of a phenomenon known as the chiral anomaly. The crucial feature, namely, the occurrence of interfaces where the Dirac mass gap changes sign, corresponds to tuning our photon band problem across a critical point using the Faraday effect.

We have shown that analogs of quantum-Hall-effect edge modes can exist in photonic crystals whose band gaps can be tuned by a Faraday coupling. The crucial new feature we present here is that photonic systems can have bands with nontrivial topological properties including nonzero Chern invariants. These in turn can be varied in a controlled manner to yield unidirectional (chiral) edge modes. The edge modes are robust against elastic backscattering since they are states that are protected by the underlying 2D band-structure topology. However, they are not robust against photon-number-nonconserving processes, such as absorption and other nonlinear effects. We believe that this could be an entirely new direction in photonic-band-structure engineering due to the absence of scattering at bends and imperfections in the channel.

While such unidirectional edge modes are usually associated with an incompressible liquid of charged fermions, we have managed to construct a means by which they also occur in photonic systems. The photonic bands will certainly not have an analog of the *bulk* physics associated with the quantum Hall effect (QHE), since there is no meaning to the notion of "filling" a photon band. Nevertheless, the topological properties of the Bloch bands which give rise to the chiral behavior of the edge modes due to the breaking of time-reversal symmetry do persist in the photonic system. While the QHE describes a ground-state property of a fermionic system, in the photonic system, the analogs of the QHE edge modes are observable when a light beam, tuned to a frequency within the bandwidth of the gap opened by the Faraday effect, is applied to the metamaterial, forming a one-way waveguide. The basic physical picture is summarized in Fig. 17.

A practical realization of such one-way transmission channels in photonics will necessarily have to deal with the problem of finding a magneto-optic material with a strong enough Faraday effect to confine the light close to the interface. Furthermore, in a practical design, the problem of TE-TM mode mixing when light is confined in the direction perpendicular to the 2D system will have to be addressed. A practical design could, for instance, make use of PBG materials to confine light in the z direction. We note that magnetic field effects are but one path toward a realization; the breaking of time-reversal symmetry, independent of the detailed mechanism, is the more fundamental requirement. Although there are many obstacles to the realization of such interesting effects in photonics, none of them are fundamental, and we believe that these unidirectional channels could have potentially useful technological applications which could in principle be realized someday through band-structure engineering.

ACKNOWLEDGMENTS

This work was supported in part by the U.S. National Science Foundation (under MRSEC Grant No. DMR-0213706 at the Princeton Center for Complex Materials). Part of this work was carried out at the Kavli Institute for Theoretical Physics, Santa Barbara, with support from KITP's NSF Grant No. PHY99-07949.

APPENDIX A: FREQUENCY DEPENDENCE OF THE DIELECTRIC MEDIA

In this appendix, we will provide the details of the generalization of the normal mode problem to include the frequency-dependent response of the media outlined in Sec. II. We shall couple the electromagnetic fields to harmonic

oscillator degrees of freedom of the medium. Defining $\phi_{i\sigma}$ and $\pi_{i\sigma}$ $(i=1,\cdots,N,\ \sigma=\epsilon,\mu)$ to be a set of N independent canonically conjugate oscillator coordinates and momenta, respectively, which represent internal polarization and magnetization modes, we consider the total Hamiltonian

$$H = H^{\mathrm{EM}} + \sum_{\sigma} H^{\sigma} \quad (\sigma = \epsilon, \mu), \tag{A1}$$

where, for instance,

$$H^{\epsilon} = \sum_{i} D^{a}[\alpha_{i\epsilon}(\boldsymbol{r})^{a}\pi_{i\epsilon}(\boldsymbol{r}) + \beta^{a}_{i\epsilon}(\boldsymbol{r})\phi_{i\epsilon}(\boldsymbol{r})] + \frac{1}{2}\sum_{i} \omega_{i\epsilon}[\pi_{i\epsilon}(\boldsymbol{r})^{2} + \phi_{i\epsilon}(\boldsymbol{r})^{2}].$$

The first term above represents the local coupling between the electric fluxes and the polarization modes, whereas the second term represents the energy of the oscillators themselves. A similar equation exists for the magnetization degrees of freedom coupled with the magnetic fluxes. The Hamiltonian, as stated in Eq. (A1), is real symmetric and positive definite, and therefore its eigenvalues are real. The electric and magnetic fields are obtained by varying the Hamiltonian with respect to the associated flux densities $E_{a}(\boldsymbol{r}) = \delta\mathcal{H}/\delta D^{a}(\boldsymbol{r})$, $H_{a}(\boldsymbol{r}) = \delta\mathcal{H}/\delta B^{a}(\boldsymbol{r})$,

$$E_{a}(\boldsymbol{r}) = \epsilon^{-1}_{ab}(\boldsymbol{r})D^{b}(\boldsymbol{r}) + \sum_{n}[\alpha^{a}_{n\epsilon}(\boldsymbol{r})\phi_{n\epsilon}(\boldsymbol{r}) + \beta^{a}_{n\epsilon}(\boldsymbol{r})\pi_{n\epsilon}(\boldsymbol{r})], \tag{A2}$$

and similarly for the field H_{a}. The time evolution of the oscillator modes is obtained from the Hamilton equations of motion (letting $\partial_{t}\phi_{n\sigma} = -i\omega\phi_{n\sigma}$, etc.),

$$-i\omega\phi_{n\epsilon}(\boldsymbol{r}) = \frac{\delta\mathcal{H}}{\delta\pi_{n\epsilon}(\boldsymbol{r})} = \omega_{n\epsilon}\pi_{n}(\boldsymbol{r}) + \beta^{a}_{n}(\boldsymbol{r})D^{a}(\boldsymbol{r}), \tag{A3}$$

$$i\omega\pi_{n\epsilon}(\boldsymbol{r}) = \frac{\delta\mathcal{H}}{\delta\phi_{n\epsilon}(\boldsymbol{r})} = \omega_{n\epsilon}\phi_{n\epsilon}(\boldsymbol{r}) + \alpha^{a}_{n\epsilon}(\boldsymbol{r})D^{a}(\boldsymbol{r}). \tag{A4}$$

We invert this equation to solve for the oscillator coordinates and momenta in terms of the fluxes:

$$\begin{pmatrix} \phi_{n\epsilon}(\boldsymbol{r}) \\ \pi_{n\epsilon}(\boldsymbol{r}) \end{pmatrix} = \frac{1}{\omega^{2} - \omega_{n}^{2}} \begin{pmatrix} \omega_{n} & i\omega \\ -i\omega & \omega_{n} \end{pmatrix} \begin{pmatrix} \alpha^{a}_{n\epsilon}(\boldsymbol{r}) \\ \beta^{a}_{n\epsilon}(\boldsymbol{r}) \end{pmatrix} D^{a}(\boldsymbol{r}). \tag{A5}$$

By substituting Eq. (A5) into the expression for the electric field (A2), we obtain a correction $\delta\epsilon^{-1}_{ab}(\boldsymbol{r},\omega)$ to the permittivity tensor coming from the oscillator modes:

$$\delta\epsilon^{-1}_{ab}(\boldsymbol{r},\omega) = \sum_{n}\left(\frac{\Gamma^{\epsilon}_{ab}(\boldsymbol{r})(\omega+\omega_{n}) - \Gamma^{*\epsilon}_{ab}(\boldsymbol{r})(\omega-\omega_{n})}{\omega^{2}-\omega_{n}^{2}}\right), \tag{A6}$$

where

$$\Gamma^{ab}_{\epsilon}(\boldsymbol{r}) = [\alpha^{a}_{n\epsilon}(\boldsymbol{r}) - i\beta^{a}_{n\epsilon}(\boldsymbol{r})][\alpha^{b}_{n\epsilon}(\boldsymbol{r}) + i\beta^{b}_{n\epsilon}(\boldsymbol{r})]. \tag{A7}$$

Finally, the correction term above to the permittivity is expressed in Kramers-Kronig form as

$$\delta\epsilon^{-1}_{ab}(\boldsymbol{r},\omega) = \sum_{n}\left(\frac{\Gamma^{\epsilon}_{ab}(\boldsymbol{r})}{\omega-\omega_{n}} - \frac{\Gamma^{\epsilon *}_{ab}(\boldsymbol{r})}{\omega+\omega_{n}}\right). \tag{A8}$$

The same formal manipulations occur in the frequency dependence of the magnetization modes; in the end, the constitutive relations are given by a tensor $B(\boldsymbol{r},\omega)$ defined by

$$B(\boldsymbol{r},\omega) = \begin{pmatrix} \epsilon^{-1}(\boldsymbol{r},\omega) & 0 \\ 0 & \mu^{-1}(\boldsymbol{r},\omega) \end{pmatrix}, \tag{A9}$$

which is written in Kramers-Kronig form as

$$B_{ab}(\boldsymbol{r},\omega) = S_{ab}(\boldsymbol{r}) + \sum_{n}\left(\frac{\Gamma_{ab}(\boldsymbol{r})}{\omega-\omega_{n}} - \frac{\Gamma^{*}_{ab}(\boldsymbol{r})}{\omega+\omega_{n}}\right). \tag{A10}$$

The first term $S_{ab}(\boldsymbol{r}) = \lim_{\omega\to\infty} B(\boldsymbol{r},\omega)$ is the same tensor defining the Hamiltonian in Eq. (14). In the zero-frequency limit,

$$B_{ab}(\boldsymbol{r},0) = S_{ab}(\boldsymbol{r}) - \sum_{n}\left(\frac{\Gamma_{ab}(\boldsymbol{r}) + \Gamma^{*}_{ab}(\boldsymbol{r})}{\omega_{n}}\right). \tag{A11}$$

The stability of the medium imposes the following important constraint:

$$B(\boldsymbol{r},0) > 0. \tag{A12}$$

Eliminating S_{ab} in Eq. (A10) using Eq. (A11), we get

$$\delta B(\omega) = \sum_{n}\left[\Gamma\left(\frac{\omega}{\omega_{n}(\omega-\omega_{n})}\right) + \Gamma^{*}\left(\frac{\omega}{\omega_{n}(\omega+\omega_{n})}\right)\right],$$

where $\delta B(\omega) = B(\omega) - B(0)$. Whereas $B(\omega)$ is not a positive-definite matrix, the quantity that is guaranteed to be positive definite in lossless frequency ranges is

$$\tilde{B}(\omega) = B(\omega) - \omega\frac{\partial}{\partial\omega}B(\omega) > 0, \tag{A13}$$

because

$$\tilde{B}(\omega) = B(0) + \sum_{n}\frac{1}{\omega_{n}}\left[\Gamma_{n}\left(\frac{\omega}{\omega-\omega_{n}}\right)^{2} + \Gamma^{*}_{n}\left(\frac{\omega}{\omega+\omega_{n}}\right)^{2}\right], \tag{A14}$$

and Γ_{n}, Γ^{*}_{n}, and $B(0)$ are all positive-definite tensors.

Although $B(\omega)$ is not positive definite, we will be interested in cases where

$$\mathrm{Det}[B(\omega)] = 0. \tag{A15}$$

When this condition is satisfied and $B(\omega)$ has no zero modes corresponding to metallic conditions, there is a well-defined inverse tensor $B^{-1}(\omega)$,

$$B^{-1}(\boldsymbol{r},\omega) = \begin{pmatrix} \epsilon(\boldsymbol{r},\omega) & 0 \\ 0 & \mu(\boldsymbol{r},\omega) \end{pmatrix}. \tag{A16}$$

From the stability condition stated for $B(\omega)$, there exists a similar condition for $B^{-1}(\omega)$:

$$B - \omega\frac{\partial}{\partial\omega}B = B\left(B^{-1} + \omega\frac{\partial}{\partial\omega}B^{-1}\right)B > 0,$$

where we have made use of $B^{-1}B=1$ and $\partial/\partial\omega(B^{-1}B)=0$. Supplementing the inequality above with the condition in Eq. (A15), we obtain

$$\tilde{B}^{-1}(\omega) \equiv \frac{\partial}{\partial\omega}[\omega B^{-1}(\omega)] > 0. \tag{A17}$$

The eigenvalue problem is solved for each value of the Bloch vector $\boldsymbol{k}$ in the first Brillouin zone, and the formal strategy for obtaining the energy eigenvalues is to solve $\boldsymbol{A}|\boldsymbol{u}_n(\boldsymbol{k})\rangle = \omega_n(\boldsymbol{k})\boldsymbol{B}^{-1}(\omega(\boldsymbol{k}))|\boldsymbol{u}_n(\boldsymbol{k})\rangle$, and then to *vary* ω until it coincides with a frequency of an eigenmode. The stability condition [see Eq. (A7)] guarantees that such a prescription enables us to find the entire spectrum in a lossless range of real frequencies, where $\tilde{B}^{-1}$ is Hermitian.

Indeed, if we consider for the moment the Hermitian problem

$$[\boldsymbol{A} - \omega\boldsymbol{B}^{-1}(\omega)]|\boldsymbol{u}_n\rangle = \lambda_n(\omega)|\boldsymbol{u}_n\rangle, \tag{A18}$$

and vary ω to find the *zero modes*

$$\lambda_n(\omega) = 0, \tag{A19}$$

the stability of such a prescription is guaranteed only if

$$\frac{\partial\lambda_n}{\partial\omega} < 0, \tag{A20}$$

so that the eigenvalues are monotonically decreasing functions of ω. But from first-order perturbation theory we know that the requirement above is satisfied only if

$$\langle\boldsymbol{u}_n|\frac{d}{d\omega}[\omega B^{-1}(\omega)]|\boldsymbol{u}_n\rangle > 0, \tag{A21}$$

which is precisely equivalent to the condition in Eq. (A17).

When we eliminate the internal oscillator (polariton) modes and explicitly substitute the expressions in Eq. (A5) into the total Hamiltonian Eq. (A1), we obtain the following quadratic form that involves only the electromagnetic flux densities:

$$H = \frac{1}{2}\sum_{ij}\tilde{B}^{-1}_{ij}(\omega)(u_i)^* u_j. \tag{A22}$$

Our result can be summarized as follows. We begin with our total Hamiltonian Eq. (A1), which can be written as a positive-definite real symmetric matrix whose states exist in an enlarged Hilbert space containing electromagnetic flux densities and internal oscillator modes. When we integrate out the nonresonant internal oscillator modes of the media, we are left with a set of effective constitutive relations of the form

$$v_{i\lambda} = \sum_j B_{ij}(\omega_\lambda)u^+_{j\lambda}e^{i\omega_\lambda t} + \text{c.c.}, \tag{A23}$$

and an effective Hamiltonian (which represents the conserved time-averaged energy density of the electromagnetic fields as well as the oscillator modes) that involves a *different* tensor $\tilde{B}_{ij}(\omega)$ given in (A22). Using the relation in Eq. (A13), we can equivalently write the Hamiltonian as

$$H = \frac{1}{2}\sum_{ij}\tilde{B}_{ij}(v_i)^* v_j. \tag{A24}$$

For the case of generalized frequency dependence considered here, the normalization of the electromagnetic fields is given (up to a scale factor) in terms of the time-averaged energy density Eq. (A22):

$$\sum_{\mu\nu}((\boldsymbol{u}_\mu)^*, \tilde{\boldsymbol{B}}^{-1}(\omega_\mu)\boldsymbol{u}_\nu) = \frac{1}{\omega_\mu}\delta_{\mu\nu}. \tag{A25}$$

Finally, the matrix $\tilde{\boldsymbol{B}}^{-1}$ and not $\boldsymbol{B}^{-1}$ enters the expression for the Berry connection, since it also defines the normalization of our states.

APPENDIX B: NUMERICAL ALGORITHMS FOR BAND-STRUCTURE CALCULATIONS

In this appendix, we shall describe our formulation of the photonic-band-structure problem, which has been used in the computations of the edge mode spectra. Since we always neglect absorption and emission and other nonlinear processes of light (i.e., we work within an approximation of photon number conservation), we seek a real-space Hamiltonian formulation of the band-structure problem. A real-space method is desirable over existing Fourier-space methods for our purposes; the modes we are particularly interested in are obtained in domain wall configurations of the Faraday mass term as a function of position, and it is most simple and suitable to work within a real-space formulation.

In the numerical implementation of a Hamiltonian formulation, we shall treat the continuum flux densities $\langle\boldsymbol{y}| = (\boldsymbol{D},\boldsymbol{B})$ rather than $\langle\boldsymbol{r}| = \langle\boldsymbol{E},\boldsymbol{H}\rangle$ as our fundamental dynamical variables. The former set obey the source-free Gauss relations

$$\boldsymbol{\nabla}\cdot|\boldsymbol{y}\rangle = 0. \tag{B1}$$

The Hamiltonian of our system is given by the following quadratic form:

$$\mathcal{H} = \frac{1}{2}(\boldsymbol{D},\epsilon^{-1}\boldsymbol{D}) + \frac{1}{2}(\boldsymbol{B},\mu^{-1}\boldsymbol{B}). \tag{B2}$$

Furthermore, the propagating solutions of Maxwell's equations require the fields to be coupled in noncanonical Poisson bracket relations:

$$\{D^a(x), B^b(x')\} = \epsilon^{abc}\boldsymbol{\nabla}_c\delta^3(x-x'). \tag{B3}$$

The two sets of fields are related by $|\boldsymbol{y}\rangle = \boldsymbol{B}|\boldsymbol{r}\rangle$, where $\boldsymbol{B}$ is the matrix of constitutive relations introduced in Sec. II. The source-free Maxwell equations are slight variants of the ones described in Sec. II, written as a generalized eigenmode problem of the form

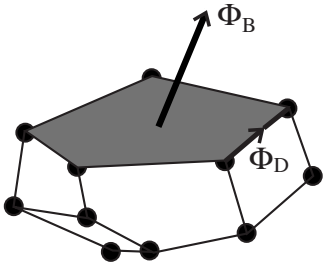

FIG. 18. The generic discretization scheme for the photon-band-structure problem. Space is broken up into polyhedra. The local electric energy density is defined at the vertices of each polyhedron, and the electric fluxes, defined on the edges of the polyhedron, connect two electric energy sites. The volume of the polyhedron is associated with local magnetic energy density, and magnetic fluxes exist on the faces of the polyhedron. The scheme here has electric-magnetic duality in that a dual polyhedron can be defined, on the vertices of which the magnetic energy density is defined, etc. The scheme here is inspired by lattice QED, which ensures the correct long-wavelength photon dispersion; the only difference here is the absence of sources.

$$\boldsymbol{A}\tilde{\boldsymbol{B}}|\boldsymbol{y}\rangle = \omega|\boldsymbol{y}\rangle. \tag{B4}$$

The matrix $\boldsymbol{A}$ is the imaginary antisymmetric matrix introduced in Sec. II, and $\tilde{\boldsymbol{B}}=\boldsymbol{B}^{-1}$ is a positive-definite Hermitian matrix. The eigenmode problem here is formally analogous to the problem of a noncanonical harmonic oscillator with Hamiltonian

$$\mathcal{H} = \frac{1}{2}\sum_{ij} \tilde{B}_{ij} y_i y_j, \tag{B5}$$

and Poisson brackets

$$\{y_i, y_j\} = A_{ij}. \tag{B6}$$

Since $\boldsymbol{A}$ is imaginary and antisymmetric, its eigenvalues are either zero or come in pairs with opposite sign. It is the presence of zero modes which prevents a canonical treatment of the problem. In the Maxwell problem, one-third of the $\boldsymbol{A}$ matrix eigenvalues are zero modes.

In the spatial discretization of this problem, we divide space into polyhedral cells, whose vertices contain the local electrical energy density as well as the inverse permittivity tensor $\epsilon_{ij}^{-1}(\boldsymbol{r})$. The electrical fluxes Φ_D are defined on the edges of the polyhedron, while the magnetic fluxes Φ_B are associated with the faces of each cell. Finally, the magnetic energy and the local inverse permeability tensor $\mu_{ij}^{-1}(\boldsymbol{r})$ are defined on the centers of each polyhedron (Fig. 18).

This discretization scheme preserves the self-duality of the source-free Maxwell equations in three dimensions. For each such electric polyhedron described above, there is a dual magnetic polyhedron whose faces correspond to the edges of the electric polyhedron, and whose center corresponds to the vertices of the electric polyhedron.

The discretized form of the $\boldsymbol{A}$ matrix couples electric fluxes to magnetic ones, and vice versa. The coupling is (see Fig. 19)

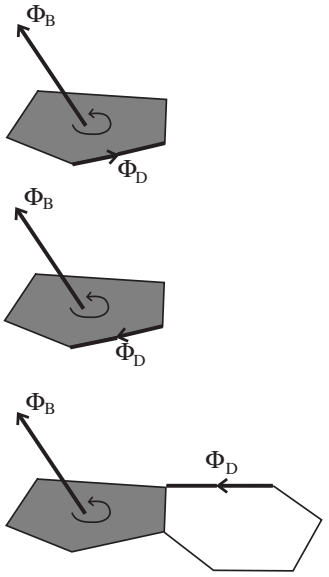

FIG. 19. The discretized form of $\boldsymbol{A}$, which contains the Poisson bracket relations of the fluxes. Shown here are example configurations of $\{\Phi_i^D, \Phi_j^B\} = +i$ (top), $-i$ (middle), and 0 (bottom).

$$A_{ij}^{DB} = \{\Phi_i^D, \Phi_j^B\} = 0, \pm i. \tag{B7}$$

The $\boldsymbol{B}$ matrix couples fluxes of the same type, and depends on the geometry of the polyhedra used to discretize space. For the case of a simple cubic discretization, and for the electric fluxes (see Fig. 20),

$$B_{ii} = \frac{1}{2}[\epsilon_{ii}^{-1}(\boldsymbol{r}_1) + \epsilon_{ii}^{-1}(\boldsymbol{r}_2)], \tag{B8}$$

$$B_{ij} = \frac{1}{4}\epsilon_{ji}^{-1}(\boldsymbol{r}_2). \tag{B9}$$

Identical relations involving the inverse permeability tensor are constructed for the magnetic fluxes. With the present formulation, the complete Hamiltonian of the system is expressed as a sum of local terms, $\mathcal{H}=\Sigma_n h(\boldsymbol{r}_n)$, with

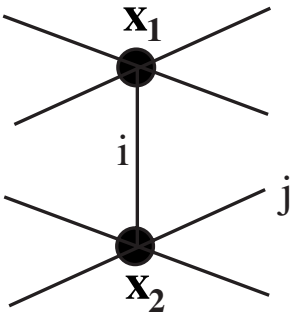

FIG. 20. The discretized form of $\boldsymbol{B}$, which contains the geometric as well as the dynamics information. It couples fluxes of the same type only, and allows for anisotropy in the constitutive relations.

$$h(\boldsymbol{r}_n) = \sum_{ij} B_{ij}(\boldsymbol{r}_n) y_i y_j. \tag{B10}$$

Using this method, we can handle the case where the constitutive relations have generalized anisotropy, and vary in space.

We have made use of a simple cubic discretization of this general algorithm (although similar implementations using bcc and fcc lattices have given the correct count of the long-wavelength photon modes) to compute photonic band structures. The fluxes Φ^D and Φ^B are made to obey the generalized Bloch boundary conditions

$$\Phi^\sigma(\boldsymbol{x}+\boldsymbol{R}) = e^{i\boldsymbol{k}\cdot\boldsymbol{R}}\Phi^\sigma(\boldsymbol{x}), \quad \sigma = D,B, \tag{B11}$$

where $\boldsymbol{R}$ is a lattice translation of the particular photonic crystal under consideration, and $\boldsymbol{k}$ is a Bloch vector in the first Brillouin zone. We compute the band structure of the system by varying the Bloch vector in the boundary conditions, which introduces Bloch phase factors into a few off-diagonal elements of the $\boldsymbol{A}$ and $\boldsymbol{B}$ matrices and gives rise to the band dispersions.

Both the $\boldsymbol{A}$ and $\boldsymbol{B}$ matrices are sufficiently sparse and are stored as matrix-vector multipliers and treated using a Lanczos algorithm. However, due to the significantly large number of zero modes, a conventional Lanczos treatment of Eq. (B4) would not converge. The Lanczos adaptation for the photonic problem is done by modifying the $\boldsymbol{A}$ matrix to

$$\boldsymbol{A} \to \boldsymbol{A}' = \boldsymbol{A}\boldsymbol{B}\boldsymbol{A} - 2\omega_0 \boldsymbol{A}, \tag{B12}$$

$$\boldsymbol{A}'\boldsymbol{B}|\boldsymbol{y}\rangle = \omega(\omega - 2\omega_0)|\boldsymbol{y}\rangle. \tag{B13}$$

Here, ω_0 is the lowest eigenvalue, and the low-lying (negative) eigenvalues of the modified problem are now the physically relevant ones, which are easily found with the Lanczos implementation. The dimensions of the matrices are $d=6N$, where N is the number of points used to discretize the constitutive relations. We have found system sizes up to 10^6 to be accessible within this approach. Furthermore, local polarization and magnetization modes can be added to the algorithm.

APPENDIX C: DERIVATION OF THE DIRAC POINT SPLITTING

In this appendix, we derive a general expression for the frequency splitting at the Dirac point caused by inversion- or time-reversal-symmetry-breaking perturbations. We will use braket notation to represent our eigenvectors instead of writing equations for each component. We suppose that we know the exact eigenstates of the problem,

$$\boldsymbol{A}|\boldsymbol{u}_0\rangle = \omega_D \boldsymbol{B}_0^{-1}|\boldsymbol{u}_0\rangle, \tag{C1}$$

and that the solutions are twofold degenerate at the Dirac point, as for example, in the numerical examples we have considered. Now add a perturbation in the constitutive relations:

$$\boldsymbol{B}^{-1} = \boldsymbol{B}_0^{-1} + \lambda \boldsymbol{B}_1^{-1}. \tag{C2}$$

This term represents our inversion- or time-reversal-symmetry-breaking perturbation. To find the splitting of the Dirac point (our "Dirac mass"), we solve the modified problem

$$\boldsymbol{A}|\boldsymbol{u}\rangle = \omega(\boldsymbol{B}_0^{-1} + \lambda \boldsymbol{B}_1^{-1})|\boldsymbol{u}\rangle. \tag{C3}$$

Since the $\boldsymbol{B}_0^{-1}$ matrix is positive definite, it has a well-defined positive-definite inverse square root matrix $\boldsymbol{B}_0^{1/2}$, and we can rewrite the unperturbed problem in the form of a conventional Hermitian eigenvalue problem,

$$\boldsymbol{B}_0^{1/2}\boldsymbol{A}\boldsymbol{B}_0^{1/2}|z_0\rangle = \omega_D|z_0\rangle, \tag{C4}$$

where

$$|z_0\rangle = \boldsymbol{B}_0^{-1/2}|\boldsymbol{u}_0\rangle. \tag{C5}$$

The new eigenvalue problem with the symmetry-breaking terms is

$$\begin{aligned}\boldsymbol{A}|\boldsymbol{u}\rangle &= \omega(\boldsymbol{B}_0^{-1} + \lambda \boldsymbol{B}_1^{-1})|\boldsymbol{u}\rangle \\ &= \omega \boldsymbol{B}_0^{-1/2}(1 + \lambda \boldsymbol{B}_0^{1/2}\boldsymbol{B}_1^{-1}\boldsymbol{B}_0^{1/2})\boldsymbol{B}_0^{-1/2}|\boldsymbol{u}\rangle,\end{aligned}$$

which subsequently is rewritten in the canonical form as

$$\boldsymbol{B}_0^{1/2}(\boldsymbol{A} - \lambda\omega \boldsymbol{B}_1^{-1})\boldsymbol{B}_0^{1/2}|z\rangle = \omega|z\rangle, \tag{C6}$$

where $|z\rangle = \boldsymbol{B}_0^{-1/2}|\boldsymbol{u}\rangle$. The correction to the spectrum to first order in perturbation theory in the eigenvalue problem above is then

$$\delta\omega = -\omega_D \lambda \langle z_0|\boldsymbol{B}_0^{1/2}\boldsymbol{B}_1^{-1}\boldsymbol{B}_0^{1/2}|z_0\rangle = -\omega_D \lambda \frac{\langle \boldsymbol{u}_0|\boldsymbol{B}_1^{-1}|\boldsymbol{u}_0\rangle}{\langle \boldsymbol{u}_0|\boldsymbol{B}_0^{-1}|\boldsymbol{u}_0\rangle}.$$

We have restored the normalization factor for the state $|\boldsymbol{u}_0\rangle$ in the last line above. Thus, our main result here is a general expression for the splitting of the Dirac point frequency spectrum, given by the dimensionless quantity

$$\frac{\delta\omega}{\omega_D} = -\lambda \frac{\langle \boldsymbol{u}_0|\boldsymbol{B}_1^{-1}|\boldsymbol{u}_0\rangle}{\langle \boldsymbol{u}_0|\boldsymbol{B}_0^{-1}|\boldsymbol{u}_0\rangle}. \tag{C7}$$

[1] J. D. Joannopoulos *et al.*, *Photonic Crystals: Molding the Flow of Light* (Princeton University Press, Princeton, NJ, 1995).

[2] R. Marques, J. Martel, F. Mesa, and F. Medina, Phys. Rev. Lett. **89**, 183901 (2002).

[3] Shawn-Yu Lin, Edmund Chow, Vince Hietala, and Pierre R. Villeneuve, Science **282**, 274 (1998).

[4] G. Sundaram and Q. Niu, Phys. Rev. B **59**, 14915 (1999).

[5] B. Simon, Phys. Rev. Lett. **51**, 2167 (1983).

[6] M. V. Berry, Proc. R. Soc. London, Ser. A **392**, 45 (1984).

[7] M. Onoda, S. Murakami, and N. Nagaosa, Phys. Rev. Lett. **93**, 083901 (2004).

[8] F. D. M. Haldane and S. Raghu, Phys. Rev. Lett. **100**, 013904

(2008).
[9] Wei-Li Lee, Satoshi Watauchi, V. L. Miller, R. J. Cava, and N. P. Ong, Science **303**, 1647 (2004).
[10] K. v. Klitzing, G. Dorda, and M. Pepper, Phys. Rev. Lett. **45**, 494 (1980).
[11] R. B. Laughlin, Phys. Rev. Lett. **50**, 1395 (1983).
[12] D. R. Hofstadter, Phys. Rev. B **14**, 2239 (1976).
[13] M. C. Chang and Q. Niu, Phys. Rev. B **53**, 7010 (1996).
[14] D. J. Thouless, M. Kohmoto, M. P. Nightingale, and M. den Nijs, Phys. Rev. Lett. **49**, 405 (1982).
[15] F. D. M. Haldane, Phys. Rev. Lett. **61**, 2015 (1988).
[16] M. Onoda and N. Nagaosa, Phys. Rev. Lett. **90**, 206601 (2003).
[17] C. L. Kane and E. J. Mele, Phys. Rev. Lett. **95**, 146802 (2005); **95**, 226801 (2005).
[18] S. Pancharatnam, Proc. Indian Acad. Sci., Sect. A **44A**, 247 (1956).
[19] R. Karplus and J. M. Luttinger, Phys. Rev. **95**, 1154 (1954).
[20] M. Kohmoto, Ann. Phys. (N.Y.) **160**, 343 (1985).
[21] R. C. Booth and E. A. D. White, J. Phys. D **17**, 579 (1984).
[22] L. D. Landau and L. P. Lifshitz, *Quantum Mechanics: Non-Relativistic Theory* (Elsevier Science, Burlington, MA, 2003).
[23] M. Plihal and A. A. Maradudin, Phys. Rev. B **44**, 8565 (1991).
[24] D. J. Thouless, *Topological Quantum Number in Nonrelativistic Physics* (World Scientific, Singapore, 1998).